

Differential decay rate of $B \rightarrow \pi l \nu$ semileptonic decay with lattice NRQCD

S. Aoki^a, M. Fukugita^b, S. Hashimoto^c, K.-I. Ishikawa^c, N. Ishizuka^{a,d}, Y. Iwasaki^{a,d},
K. Kanaya^{a,d}, T. Kaneko^c, Y. Kuramashi^c, M. Okawa^c, T. Onogi^{e,f}, S. Tominaga^d,
N. Tsutsui^c, A. Ukawa^{a,d}, N. Yamada^c, T. Yoshie^{a,d}

^a*Institute of Physics, University of Tsukuba, Tsukuba 305-8571, Japan*

^b*Institute for Cosmic Ray Research, University of Tokyo, Kashiwa 277-8582, Japan*

^c*High Energy Accelerator Research Organization (KEK), Tsukuba 305-0801, Japan*

^d*Center for Computational Physics, University of Tsukuba, Tsukuba 305-8571, Japan*

^e*Department of Physics, Hiroshima University, Higashi-Hiroshima 739-8526, Japan**

^f *Yukawa Institute for Theoretical Physics, Kyoto University, Kyoto 606-8502, Japan[†]*

(August 17, 2019)

Abstract

We present a lattice QCD calculation of $B \rightarrow \pi l \nu$ semileptonic decay form factors in the small pion recoil momentum region. The calculation is performed on a quenched $16^3 \times 48$ lattice at $\beta = 5.9$ with the NRQCD action including the full $1/M$ terms. The form factors $f_1(v \cdot k_\pi)$ and $f_2(v \cdot k_\pi)$ defined in the heavy quark effective theory for which the heavy quark scaling is manifest are adopted, and we find that the $1/M$ correction to the scaling is small for the B meson. The dependence of form factors on the light quark mass and on the recoil energy is found to be mild, and we use a global fit of the form factors at various quark masses and recoil energies to obtain model independent results for the physical differential decay rate. We find that the B^* pole contribution dominates the form factor $f^+(q^2)$ for small pion recoil energy, and obtain the differential decay rate integrated over the kinematic region $q^2 > 18 \text{ GeV}^2$ to be $|V_{ub}|^2 \times (1.18 \pm 0.37 \pm 0.08 \pm 0.31) \text{ psec}^{-1}$, where the first error is statistical, the second is that from perturbative calculation, and the third is the systematic error from finite lattice spacing and the chiral extrapolation. We also discuss the systematic errors in the soft pion limit for

*address before April, 2001

[†]address since April, 2001

$f^0(q_{max}^2)$ in the present simulation.

PACS number(s): 12.38.Gc, 12.39.Hg, 13.20.He, 14.40.Nd

I. INTRODUCTION

The exclusive decay modes $B^0 \rightarrow \pi^- l^+ \nu_l$ and $B^0 \rightarrow \rho^- l^+ \nu$ may provide us with the best experimental input to determine the Cabibbo-Kobayashi-Maskawa (CKM) matrix element $|V_{ub}|$. At present these decays are measured by CLEO [1,2] with error of order 20%. A prerequisite for the determination of $|V_{ub}|$ is an accurate calculation of the form factors involved in these semileptonic decays, but the theoretical prediction of the form factors for the entire kinematical range is still difficult. However, with the advent of the B factories, BaBar, Belle and CLEO III, we expect that the differential decay rate will be measured precisely as a function of momentum transfer q^2 in near future. This means that to determine $|V_{ub}|$ we do not necessarily need the form factor for the entire kinematic region of q^2 , but calculations in a certain limited range of q^2 will practically suffice.

Lattice QCD provides a promising framework to compute the form factors without resorting to specific phenomenological models. Exploratory studies have already been made by a few groups [3–5], but more extensive studies are clearly needed to provide realistic predictions. In this work we attempt to compute the form factors and differential decay rates of $B \rightarrow \pi l \nu$ for the momentum range $q^2 > 18 \text{ GeV}^2$, which is set by the condition that the spatial momenta of the initial and final hadrons be much smaller than the lattice cutoff $1/a$, $|\mathbf{k}| \ll 1/a \simeq 2 \text{ GeV}/c$, to avoid discretization error.

An important point in the calculation of the B meson matrix elements is to reduce the systematic error arising from a heavy quark mass M which is larger than $1/a$. One approach adopted in the literature is to calculate the matrix elements with a relativistic action for heavy quarks around the charm quark mass and to extrapolate them to the bottom quark mass. Although this approach seems to work reasonably well in the recent studies of $B \rightarrow \pi l \nu$ form factors [6,7], the systematic error is magnified in the extrapolation and the heavy quark mass dependence would not be correctly predicted. This problem can be avoided by using a variant of the Heavy Quark Effective Theory (HQET), in which the heavy quark is treated non-relativistically.

A natural implementation of the idea of HQET on the lattice is the non-relativistic QCD (NRQCD) [8], which we employ in this work. With the NRQCD action the heavy quark mass dependence of the form factors can be reliably calculated [9], since the action is written as an expansion in terms of inverse heavy quark mass and higher order terms can optionally be included to achieve desired accuracy. In the $B \rightarrow \pi l \nu$ decay near zero recoil of the pion, we find that the heavy quark expansion converges well at the next-to-leading order in $1/M$.

An alternative implementation of the HQET is the Fermilab formalism [10], in which results from the conventional relativistic lattice action are reinterpreted in terms of a non-relativistic effective Hamiltonian. This formalism shares an advantage similar to that of NRQCD, and has recently been applied to a $B \rightarrow \pi l \nu$ decay calculation [11].

In the application of the HQET to the $B \rightarrow \pi l \nu$ decay, it is more natural to work with the form factors $f_1(v \cdot k_\pi)$ and $f_2(v \cdot k_\pi)$ [12], where v^μ is a heavy quark velocity and k_π^μ is a four-momentum of pion, rather than the conventional $f^+(q^2)$ and $f^0(q^2)$. This is because the argument $v \cdot k_\pi$, which is the energy of the pion in B meson rest frame, is well-defined in the limit of infinitely heavy quark mass, and the heavy quark scaling, *i.e.* $f_{1,2}(v \cdot k_\pi) \rightarrow \text{constant}$ as $M \rightarrow \infty$, is manifest in the new set of the form factors.

We calculate $f_{1,2}(v \cdot k_\pi)$ using the NRQCD action on a quenched lattice of size $16^3 \times 48$ at

$\beta = 5.9$ corresponding to $1/a \approx 1.6$ GeV. The action we use includes the full terms of order $1/M$. The $O(a)$ -improved Wilson fermion action is used for the light quark. We prepare a large statistical sample, accumulating 2,150 gauge configurations to reduce statistical noise which becomes large for states with finite momenta. This enables us to obtain good signals for the form factors for a finite spatial momentum of the pion.

This paper is organized as follows. In the next section we briefly review the definition of the HQET motivated form factors $f_{1,2}(v \cdot k_\pi)$ of Burdman *et al.* [12] and their relation to the conventional form factors. We summarize the definition of the NRQCD action in Section III, and discuss matching of the heavy-light vector current on the lattice with that in the continuum in Section IV. We describe our lattice calculation in Section V, and the results are presented in Section VI. Section VII is given to a comparison with other lattice calculations, and phenomenological implications are discussed in Section VIII. Our conclusions are presented in Section IX.

II. THE HQET FORM FACTORS FOR $B \rightarrow \pi L \nu$

The matrix element $\langle \pi(k_\pi) | \bar{q} \gamma_\mu b | B(p_B) \rangle$ for the heavy-to-light semileptonic decay $B \rightarrow \pi L \nu$ is usually parameterized as

$$\langle \pi(k_\pi) | \bar{q} \gamma^\mu b | B(p_B) \rangle = f^+(q^2) \left[(p_B + k_\pi)^\mu - \frac{m_B^2 - m_\pi^2}{q^2} q^\mu \right] + f^0(q^2) \frac{m_B^2 - m_\pi^2}{q^2} q^\mu, \quad (2.1)$$

with p_B and k_π the momenta of the initial and final pseudo-scalar mesons and $q = p_B - k_\pi$. When lepton mass is negligible, the momentum transfer q^2 ranges from 0 to $q_{max}^2 = (m_B - m_\pi)^2$. From the kinematics

$$E_\pi = v \cdot k_\pi = \frac{m_B^2 - m_\pi^2 - q^2}{2m_B}, \quad (2.2)$$

where $v = p_B/m_B$ is the four-velocity of the initial B meson, a low q^2 corresponds to a large recoil momentum of pion, for which the lattice calculation is not easy. In the other limit $q^2 \sim q_{max}^2$, however, the energy of the pion E_π in the B meson rest frame is minimum, so that spatial momenta of the initial and final hadrons are small compared to the lattice cutoff, and the lattice calculation will give a reliable answer.

In HQET, it is more natural to use v^μ and k_π^μ as independent four-vectors rather than p_B^μ and k_π^μ . Burdman *et al.* [12] defined the form factors $f_1(v \cdot k_\pi)$ and $f_2(v \cdot k_\pi)$ by

$$\langle \pi(k_\pi) | \bar{q} \gamma^\mu b | B(v) \rangle = 2 \left[f_1(v \cdot k_\pi) v^\mu + f_2(v \cdot k_\pi) \frac{k_\pi^\mu}{v \cdot k_\pi} \right], \quad (2.3)$$

where the heavy meson field is normalized with the factor $2v^0$ instead of the usual $2p_B^0$, so that $\sqrt{m_B} |B(v)\rangle = |B(p_B)\rangle$. The new form factors are functions of $v \cdot k_\pi$ and defined over the range $[m_\pi, (m_B^2 - m_\pi^2)/2m_B]$. As seen from definition (2.3) there is no explicit dependence on the heavy meson mass. Therefore, heavy quark scaling as $M \rightarrow \infty$ is manifest, namely, $f_{1,2}(v \cdot k_\pi)$ become independent of M up to logarithms arising from the renormalization of the heavy-light current. Finite M corrections are given as a power series in $1/M$.

The relation between the two definitions of form factors is given by

$$f^+(q^2) = \sqrt{m_B} \left\{ \frac{f_2(v \cdot k_\pi)}{v \cdot k_\pi} + \frac{f_1(v \cdot k_\pi)}{m_B} \right\}, \quad (2.4)$$

$$f^0(q^2) = \frac{2}{\sqrt{m_B}} \frac{m_B^2}{m_B^2 - m_\pi^2} \left\{ [f_1(v \cdot k_\pi) + f_2(v \cdot k_\pi)] - \frac{v \cdot k_\pi}{m_B} \left[f_1(v \cdot k_\pi) + \frac{m_\pi^2}{(v \cdot k_\pi)^2} f_2(v \cdot k_\pi) \right] \right\}. \quad (2.5)$$

This indicates that $f^+(q^2)$ and $f^0(q^2)$ scale in the heavy quark limit as

$$f^+(q^2) \sim \sqrt{m_B}, \quad (2.6)$$

$$f^0(q^2) \sim \frac{1}{\sqrt{m_B}}, \quad (2.7)$$

if $v \cdot k_\pi$ is kept fixed.

In the soft pion limit $k_\pi \rightarrow 0$ and $m_\pi \rightarrow 0$, we obtain simpler relations

$$f^+(q^2) \simeq \sqrt{m_B} \frac{f_2(v \cdot k_\pi)}{v \cdot k_\pi}, \quad (2.8)$$

$$f^0(q^2) \simeq \frac{2}{\sqrt{m_B}} [f_1(v \cdot k_\pi) + f_2(v \cdot k_\pi)], \quad (2.9)$$

from (2.4) and (2.5). The soft pion theorem implies that the scalar form factor $f^0(q^2)$ and the B meson leptonic decay constant f_B are related as $f^0(q_{max}^2) = f_B/f_\pi$, which means

$$f_1(0) + f_2(0) = \frac{f_B \sqrt{m_B}}{2f_\pi}. \quad (2.10)$$

The vector form factor $f^+(q^2)$ may be evaluated using the heavy meson chiral lagrangian approach [13], in which the B^* pole contributes through a $B^* B \pi$ coupling. One obtains the relation

$$\lim_{v \cdot k_\pi \rightarrow 0} f_2(v \cdot k_\pi) = g \frac{f_{B^*} \sqrt{m_{B^*}}}{2f_\pi} \frac{v \cdot k_\pi}{v \cdot k_\pi + \Delta_B}, \quad (2.11)$$

where the vector meson decay constant f_{B^*} is defined by $\langle 0 | V^\mu | B^*(p) \rangle = i f_{B^*} m_{B^*} \epsilon^\mu(p)$, and g denotes the $B^* B \pi$ coupling. The B^* propagator gives a factor $1/(v \cdot k_\pi + \Delta_B)$, in which $\Delta_B = m_{B^*} - m_B$. Since the hyperfine splitting $\Delta_B \approx 46$ MeV is much smaller than the ‘pion’ mass, we consider in the lattice simulation that (2.11) depends little on $v \cdot k_\pi$. This behavior of f_2 is actually found in our simulation. Equation (2.11) leads to the well-known vector meson dominance form for the form factor $f^+(q^2)$

$$\lim_{q^2 \rightarrow m_B^2} f^+(q^2) = \frac{f_{B^*}}{f_\pi} \frac{g}{1 - q^2/m_{B^*}^2}, \quad (2.12)$$

which is also reproduced in our calculation.

III. LATTICE NRQCD

We use the NRQCD formalism defined on the lattice [8] to treat the heavy b quark without large discretization errors increasing as a power of aM . NRQCD is designed to approximate non-relativistic motion of heavy quark inside hadrons, and is expressed as a systematic expansion in some small parameter depending on the hadron considered. For the heavy-light meson system such as the B meson, the expansion parameter is given by Λ_{QCD}/M , with Λ_{QCD} the typical momentum scale of QCD $\sim 300\text{--}500$ MeV. At the next-to-leading order in Λ_{QCD}/M , the lagrangian in the continuum Euclidean space-time is written as

$$\mathcal{L}_{NRQCD}^{cont} = Q^\dagger \left[D_0 + \frac{\mathbf{D}^2}{2M} + g \frac{\boldsymbol{\sigma} \cdot \mathbf{B}}{2M} \right] Q, \quad (3.1)$$

for heavy quark field Q represented by a two-component non-relativistic spinor. The derivatives D_0 and \mathbf{D} are temporal and spatial covariant derivatives respectively. The leading order term D_0 represents a heavy quark as a static color source. The leading correction of order Λ_{QCD}/M comes from $\mathbf{D}^2/2M$, which gives a non-relativistic kinetic term of heavy quark. Another contribution of order Λ_{QCD}/M is the spin-(chromo)magnetic interaction $\boldsymbol{\sigma} \cdot \mathbf{B}/2M$, where \mathbf{B} denotes a chromomagnetic field strength. In the usual HQET approach, only the leading terms are present in the effective lagrangian and corrections of order Λ_{QCD}/M is incorporated when one evaluates a matrix element $\langle \mathcal{O} \rangle$ of some operator \mathcal{O} by including terms such as $\langle T \mathcal{O} \int d^4x Q^\dagger (\mathbf{D}^2/2M) Q \rangle$. In contrast, in the NRQCD approach we include the correction terms in the lagrangian (3.1) and evaluate the matrix elements with the heavy quark propagator including the effect of order Λ_{QCD}/M .

An important limitation of the NRQCD lagrangian (3.1) is that the heavy quark expansion is made in the rest frame of a heavy quark. Since the expansion parameter is p/M , where p is a typical spatial momentum of heavy quark, the lagrangian is valid only in the region where the heavy quark does not have momentum greater than $O(\Lambda_{QCD})$. Therefore, in the study of the heavy-to-light decay, the momentum of initial B meson must be small enough. Although it is possible to construct the action expanded around a finite heavy quark velocity, the heavy quark velocity is renormalized by radiative correction since the lattice violates Lorentz symmetry [14,15], which gives rise to an additional important systematic corrections. We, therefore, do not take this strategy and consider the discretization of the Lagrangian (3.1).

The lattice NRQCD action we use in this work is

$$S_{NRQCD} = \sum_{x,y} Q^\dagger(x) (\delta_{x,y} - K_Q(x,y)) Q(y) + \sum_{x,y} \chi^\dagger(x) (\delta_{x,y} - K_\chi(x,y)) \chi(y). \quad (3.2)$$

In addition to the non-relativistic heavy quark field Q , we write the term for the anti-particle field χ for completeness. The kernels to describe the time evolution of heavy quark are given by

$$K_Q(x,y) = \left[\left(1 - \frac{aH_0}{2n}\right)^n \left(1 - \frac{a\delta H}{2}\right) \delta_4^{(-)} U_4^\dagger \left(1 - \frac{a\delta H}{2}\right) \left(1 - \frac{aH_0}{2n}\right)^n \right] (x,y), \quad (3.3)$$

$$K_\chi(x,y) = \left[\left(1 - \frac{aH_0}{2n}\right)^n \left(1 - \frac{a\delta H}{2}\right) \delta_4^{(+)} U_4 \left(1 - \frac{a\delta H}{2}\right) \left(1 - \frac{aH_0}{2n}\right)^n \right] (x,y), \quad (3.4)$$

where n denotes a stabilization parameter introduced in order to remove an instability arising from unphysical momentum modes in the evolution equation [8]. The operator $\delta_4^{(\pm)}$ is defined as $\delta_4^{(\pm)}(x, y) \equiv \delta_{x_4 \pm 1, y_4} \delta_{\mathbf{x}, \mathbf{y}}$, and H_0 and δH are lattice Hamiltonians defined by

$$H_0 \equiv -\frac{\Delta^{(2)}}{2aM_0}, \quad (3.5)$$

$$\delta H \equiv -c_B \frac{g}{2aM_0} \boldsymbol{\sigma} \cdot \mathbf{B}, \quad (3.6)$$

where $\Delta^{(2)} \equiv \sum_{i=1}^3 \Delta_i^{(2)}$ is a Laplacian defined on the lattice through $\Delta_i^{(2)}$, the second symmetric covariant differentiation operator in the spatial direction i . In (3.6) the chromomagnetic field \mathbf{B} is the usual clover-leaf type lattice field strength [8]. In these definitions, the lattice operators $\Delta_i^{(2)}$ and \mathbf{B} are dimensionless, *i.e.* appropriate powers of a are understood. The space-time indices x and y are implicit in these expressions. The bare heavy quark mass M_0 is distinguished from the renormalized one M .

The lattice action (3.2) describes continuum NRQCD (3.1) in the limit of vanishing lattice spacing a at tree level. In the presence of radiative correction, however, power divergence of form $\alpha_s^n / (aM_0)^m$ with positive integers n, m can appear. This is due to the fact that NRQCD is not renormalizable, and the action should be considered as an effective theory valid for small $1/(aM_0)$. This means that the parameters in the lattice action (3.2) should be tuned to reproduce the same low energy amplitude as the continuum QCD up to some higher order corrections. One may use perturbation theory to achieve this tuning. For example, one-loop calculation of energy shift and mass renormalization was carried out for lattice NRQCD by Davies and Thacker [16] and by Morningstar [17] sometime ago, and then by ourselves [18–20] for the above particular form of the NRQCD action.¹ To improve the perturbative expansion we utilize the tadpole improvement procedure where all the gauge links in the action (3.2) are divided by its mean field value u_0 determined from the plaquette expectation value as $u_0 \equiv (\langle \text{Tr} U_P \rangle / 3)^{1/4}$. This tadpole improvement will give rise to $O(g^2)$ counter terms in the Feynman rules. The one-loop tuning of the coupling constant c_B in front of the spin-(chromo)magnetic interaction term (3.6) has not yet been performed. We, therefore, use the tree level value $c_B=1$ after making the tadpole improvement.

The relativistic four-component Dirac spinor field h is related to the two-component non-relativistic field Q and χ appearing in the NRQCD action (3.2) via the Foldy-Wouthuysen-Tani (FWT) transformation

$$h = \left(1 - \frac{\boldsymbol{\gamma} \cdot \boldsymbol{\nabla}}{2aM_0} \right) \begin{pmatrix} Q \\ \chi^\dagger \end{pmatrix}, \quad (3.7)$$

where $\boldsymbol{\nabla}$ is a symmetric covariant differentiation operator in a spatial direction.

¹ We note that the evolution kernels (3.3) and (3.4) are slightly different from the definition used, for example, in [17], where the $(1 - aH_0/2n)^n$ terms appear inside of the $(1 - a\delta H/2)$ terms.

IV. MATCHING OF THE HEAVY-LIGHT CURRENT

Since we use the lattice NRQCD action of the previous section, the continuum heavy-light vector current $\bar{q}\gamma_\mu b$ in (2.1) must be written in terms of the corresponding operator constructed with the lattice NRQCD heavy quark field h . This matching of the continuum and lattice operators has been calculated using the one-loop perturbation theory by Morningstar and Shigemitsu [21,22]. In this section we summarize their results and specify our notations.

In the one-loop matching of the continuum operator to the lattice operators, we have to consider dimension-four operators in addition to the leading dimension three operator $\bar{q}\gamma_\mu h$, in order to remove the error of order $\alpha_s \Lambda_{QCD}/M$ and $\alpha_s a \Lambda_{QCD}$. The former is the radiative correction to the FWT transformation (3.7) and the latter appears in the $O(a)$ -improvement of the lattice discretized operator. Thus the following operators are involved in the calculation.

$$V_4^{(0)} = \bar{q}\gamma_4 h, \quad (4.1)$$

$$V_4^{(1)} = -\frac{1}{2aM_0} \bar{q}\gamma_4 \gamma \cdot \nabla h, \quad (4.2)$$

$$V_4^{(2)} = -\frac{1}{2aM_0} \bar{q}\gamma \cdot \overleftarrow{\nabla} h, \quad (4.3)$$

$$V_k^{(0)} = \bar{q}\gamma_k h, \quad (4.4)$$

$$V_k^{(1)} = -\frac{1}{2aM_0} \bar{q}\gamma_k \gamma \cdot \nabla h, \quad (4.5)$$

$$V_k^{(2)} = -\frac{1}{2aM_0} \bar{q}\gamma \cdot \overleftarrow{\nabla} \gamma_4 \gamma_k h, \quad (4.6)$$

$$V_k^{(3)} = -\frac{1}{2aM_0} \bar{q}\gamma_4 \nabla_k h, \quad (4.7)$$

$$V_k^{(4)} = \frac{1}{2aM_0} \bar{q} \overleftarrow{\nabla}_k \gamma_4 h. \quad (4.8)$$

The heavy quark field h is obtained from the two-component field Q through the FWT transformation (3.7).² For the light quark q we employ the $O(a)$ -improved Wilson fermion [23].

The one-loop matching is given by

$$V_4^{cont} = \left(1 + \alpha_s \left[\frac{1}{\pi} \ln(aM_0) + \rho_{V_4}^{(0)}\right]\right) V_4^{(0)} + \alpha_s \rho_{V_4}^{(1)} V_4^{(1)} + \alpha_s \rho_{V_4}^{(2)} V_4^{(2)}, \quad (4.9)$$

$$V_k^{cont} = \left(1 + \alpha_s \left[\frac{1}{\pi} \ln(aM_0) + \rho_{V_k}^{(0)}\right]\right) V_k^{(0)} + \alpha_s \rho_{V_k}^{(1)} V_k^{(1)} + \alpha_s \left[\frac{4}{\pi} \ln(aM_0) + \rho_{V_k}^{(2)}\right] V_k^{(2)} + \alpha_s \rho_{V_k}^{(3)} V_k^{(3)} + \alpha_s \left[-\frac{4}{3\pi} \ln(aM_0) + \rho_{V_k}^{(4)}\right] V_k^{(4)}, \quad (4.10)$$

² In the definition used in [22] the heavy quark field before the FWT transformation $(Q \ 0)^T$ appears in the definition of operators. Matching coefficients for $V_4^{(1)}$ and $V_k^{(1)}$ must be converted when we use the above definition.

and the numerical coefficients $\rho_{V_4}^{(i)}$ and $\rho_{V_4}^{(k)}$ are summarized in Tables I and II for several values of aM_0 .

As we mentioned earlier, the NRQCD action employed in this work is slightly different from that of Morningstar and Shigemitsu [22]. We have therefore independently calculated the wave function renormalization and the vertex correction for the temporal component V_4 , and found that the difference of the finite constants ρ 's between the two actions is small, *e.g.*, $\sim 4\text{--}9\%$ for the vertex correction. Therefore, for the spatial vector current, for which the one-loop calculation with our action is missing, we adopt the coefficients of [22] assuming that the error is negligible. In Table I the results of our calculation for $\rho_{V_4}^{(i)}$ are listed, while results for $\rho_{V_k}^{(i)}$ in [22] are interpolated in aM_0 and given in Table II for our parameter values.

V. LATTICE CALCULATION

A. Lattice setup

Our quenched lattice calculation is carried out on a $16^3 \times 48$ lattice at $\beta = 5.9$ with the standard plaquette action for gluons. The inverse lattice spacing $1/a$ determined from the string tension is $a^{-1} = 1.64$ GeV. The scaling violation has been found to be small for our choice of the heavy and light quark actions over $1/a \simeq 1 - 2.5$ GeV in the heavy-light decay constant [19].

The parameters we choose for the heavy and light quarks are a subset of those simulated in [19]. We take four values of the bare mass aM_0 , 1.3, 2.1, 3.0 and 5.0 for the heavy quark, over a range of the physical heavy quark mass between 2 and 8 GeV. The stabilization parameter n is set to 3 (for $aM_0=1.3$ and 2.1) or 2 (for $aM_0=3.0$ and 5.0) so as to satisfy the stability condition $n > 3/(aM_0)$. We use the $O(a)$ -improved Wilson action for the light quark with the clover coefficient $c_{\text{sw}}=1.580$, which is evaluated at one-loop with the tadpole improvement. Four values 0.13630, 0.13711, 0.13769 and 0.13816 are chosen for the hopping parameters in our simulation, where the critical value κ_c is 0.13901.

We accumulate 2150 quenched configurations to reduce the statistical error for matrix elements with finite spatial momenta. Each configuration is separated by 1000 pseudo-heat-bath sweeps after 10 000 sweeps for thermalization and fixed to the Coulomb gauge. As we will see, even with this large number of statistics, signals for heaviest heavy quark or lightest light quark are not clean enough to extract the ground state.

B. Correlators

The form factors are extracted from measurements of three-point correlators

$$C^{\pi^S V_\mu^{(i)} B^S}(t_\pi, t, t_B; \mathbf{q}, \mathbf{p}_B) = \sum_{\mathbf{x}, \mathbf{y}} e^{-i\mathbf{q} \cdot \mathbf{x}} e^{i\mathbf{p}_B \cdot \mathbf{y}} \langle \mathcal{O}_\pi^S(t_\pi, \mathbf{0}) V_\mu^{(i)}(t, \mathbf{x}) \mathcal{O}_B^{S\dagger}(t_B, \mathbf{y}) \rangle, \quad (5.1)$$

of the vector currents (4.1)–(4.8) with the initial B meson and daughter pion interpolating fields \mathcal{O}_B^S and \mathcal{O}_π^S , respectively. The interpolating fields are defined by

$$\mathcal{O}_\pi^L(t, \mathbf{x}) = \bar{q}(t, \mathbf{x}) \gamma_5 q(t, \mathbf{x}), \quad (5.2)$$

$$\mathcal{O}_\pi^S(t, \mathbf{x}) = \left[\sum_{\mathbf{r}} \phi_l(|\mathbf{r}|) \bar{q}(t, \mathbf{x} + \mathbf{r}) \right] \gamma_5 \left[\sum_{\mathbf{r}'} \phi_l(|\mathbf{r}'|) q(t, \mathbf{x} + \mathbf{r}') \right], \quad (5.3)$$

$$\mathcal{O}_B^L(t, \mathbf{x}) = \bar{q}(t, \mathbf{x}) \gamma_5 h(t, \mathbf{x}), \quad (5.4)$$

$$\mathcal{O}_B^S(t, \mathbf{x}) = \bar{q}(t, \mathbf{x}) \gamma_5 \left[\sum_{\mathbf{r}} \phi_h(|\mathbf{r}|) h(t, \mathbf{x} + \mathbf{r}) \right], \quad (5.5)$$

where the operators with superscript L represent a local field, while the smeared operators defined on the Coulomb gauge fixed configurations are labeled with S . The smearing functions $\phi_l(r)$ and $\phi_h(r)$ are parameterized by $\phi_l(r) = \exp(-a_l r^{b_l})$ and $\phi_h(r) = \exp(-a_h r^{b_h})$, with parameters $a_{l,h}$ and $b_{l,h}$ determined from a measurement of light-light and heavy-light meson wave functions [19]. The wave function of the light-light meson $\phi_l(r)$ is almost independent of the light quark mass, and we use $(a_l, b_l) = (0.27, 1.13)$. The wave function describing the spread of heavy-light meson $\phi_h(r)$, on the other hand, depends significantly on the heavy quark mass, *i.e.* b_h becomes larger as heavy quark mass increases. The numerical values of (a_h, b_h) are given in Table III.

The B meson interpolating field \mathcal{O}_B^S is fixed at the time slice $t_B=24$. The light quark propagator corresponding to the spectator quark is solved for a smeared source at t_B , and the source method is used at the time slice $t_\pi=0$ to obtain the daughter light quark propagator with momentum insertion $-\mathbf{q}$. The heavy-light current is then constructed at t , which is in a region $t_\pi < t < t_B$, with the daughter light quark propagating from t_π and a heavy anti-quark evolving back from t_B . Another momentum \mathbf{p}_B is inserted at t . With this combination of momenta, the initial B meson has momentum \mathbf{p}_B and the final pion travels with momentum $\mathbf{k}_\pi = \mathbf{p}_B - \mathbf{q}$, since the fixed source at t_B emits a heavy-light meson with any momentum. The momentum combinations measured in our simulation is summarized in Table IV. Since the statistical noise grows exponentially as $\exp((E(p^2) - E(0))t)$ for the finite momentum state with energy $E(p^2)$, the spatial momentum one can measure with reasonable signal is rather limited. In fact, even in our high statistics data, the maximum momentum we could take is $(1, 0, 0)$ in unit of $2\pi/La$ as we shall discuss in the following sections.

The three-point function (5.1) is dominated by the ground state contribution for large enough separation of operators $t_\pi \ll t \ll t_B$

$$C^{\pi^S V_\mu^{(i)BS}}(t_\pi, t, t_B; \mathbf{q}, \mathbf{p}_B) \rightarrow \frac{Z_\pi^S(\mathbf{k}_\pi)}{2E_\pi(\mathbf{k}_\pi)} \frac{Z_B^S(\mathbf{p}_B)}{2E_B(\mathbf{p}_B)} \langle \pi(k_\pi) | V_\mu^{(i)} | B(p_B) \rangle, \\ \times \exp(-E_\pi(\mathbf{k}_\pi)(t - t_\pi) - E_{\text{bind}}(\mathbf{p}_B)(t_B - t)). \quad (5.6)$$

The overlap amplitudes $Z_\pi^S(\mathbf{k}_\pi)$ and $Z_B^S(\mathbf{p}_B)$ of the interpolating operators with the corresponding ground state are evaluated from the two-point correlators defined by

$$C^{\pi^S \pi^S}(t_\pi, t; \mathbf{k}_\pi) = \sum_{\mathbf{x}} e^{i\mathbf{k}_\pi \cdot \mathbf{x}} \langle \mathcal{O}_\pi^S(t_\pi, \mathbf{0}) \mathcal{O}_\pi^{S\dagger}(t, \mathbf{x}) \rangle \rightarrow \frac{Z_\pi^S(\mathbf{k}_\pi)^2}{2E_\pi(\mathbf{k}_\pi)} e^{-E_\pi(\mathbf{k}_\pi)(t - t_\pi)}, \quad (5.7)$$

$$C^{\pi^S \pi^L}(t_\pi, t; \mathbf{k}_\pi) = \sum_{\mathbf{x}} e^{i\mathbf{k}_\pi \cdot \mathbf{x}} \langle \mathcal{O}_\pi^S(t_\pi, \mathbf{0}) \mathcal{O}_\pi^{L\dagger}(t, \mathbf{x}) \rangle \rightarrow \frac{Z_\pi^S(\mathbf{k}_\pi) Z_\pi^L(\mathbf{k}_\pi)}{2E_\pi(\mathbf{k}_\pi)} e^{-E_\pi(\mathbf{k}_\pi)(t - t_\pi)}, \quad (5.8)$$

$$C^{B^S B^S}(t, t_B; \mathbf{p}_B) = \sum_{\mathbf{x}} e^{-i\mathbf{p}_B \cdot \mathbf{x}} \langle \mathcal{O}_B^S(t, \mathbf{x}) \mathcal{O}_B^{S\dagger}(t_B, \mathbf{0}) \rangle \rightarrow \frac{Z_B^S(\mathbf{p}_B)^2}{2E_B(\mathbf{p}_B)} e^{-E_{\text{bind}}(\mathbf{p}_B)(t_B - t)}, \quad (5.9)$$

$$C^{B^L B^S}(t, t_B; \mathbf{p}_B) = \sum_{\mathbf{x}} e^{-i\mathbf{p}_B \cdot \mathbf{x}} \langle \mathcal{O}_B^L(t, \mathbf{x}) \mathcal{O}_B^{S\dagger}(t_B, \mathbf{0}) \rangle \rightarrow \frac{Z_B^S(\mathbf{p}_B) Z_B^L(\mathbf{p}_B)}{2E_B(\mathbf{p}_B)} e^{-E_{\text{bind}}(\mathbf{p}_B)(t_B - t)}. \quad (5.10)$$

The ground state energy of the heavy-light meson $E_{\text{bind}}(\mathbf{p}_B)$ represents a “binding energy”, as the bare heavy quark mass is subtracted in the NRQCD formalism. In the state normalization in (5.6) and in (5.9)–(5.10), on the other hand, the heavy-light meson energy $E_B(\mathbf{p}_B)$ including the bare heavy quark mass enters in the denominator.

In practice, we calculate a ratio $R^{V_\mu^{(i)}}(t, \mathbf{k}_\pi, \mathbf{p}_B)$ of the three-point and the two-point functions

$$R^{V_\mu^{(i)}}(t; \mathbf{k}_\pi, \mathbf{p}_B) = \frac{C^{\pi^S V_\mu^{(i)} B^S}(t_\pi, t, t_B; \mathbf{q}, \mathbf{p}_B)}{C^{\pi^S \pi^L}(t_\pi, t; \mathbf{k}_\pi) C^{B^L B^S}(t, t_B; \mathbf{p}_B)} \rightarrow \frac{\langle \pi(k_\pi) | V_\mu^{(i)} | B(p_B) \rangle}{Z_\pi^L(\mathbf{k}_\pi) Z_B^L(\mathbf{p}_B)}, \quad (5.11)$$

which becomes constant in the asymptotic limit. The overlap amplitudes with the smeared interpolating fields $Z_\pi^S(\mathbf{k}_\pi)$ and $Z_B^S(\mathbf{p}_B)$ cancel between the numerator and the denominator. Typical examples of the ratio $R^{V_\mu^{(i)}}(t; \mathbf{k}_\pi, \mathbf{p}_B)$ is plotted in Figure 1, in which the data at $\kappa=0.13711$ and $aM_0=3.0$ are shown for five choices of the momentum combinations. For all these plots we find clear plateau in the large t region, where the current is closer to the B meson interpolating field than to the pion. This is due to the fact that the smearing with the measured wave function works better for heavy-light than for light-light meson, because the heavy-light system is less relativistic and the description with the wave function is more appropriate. The fit result is indicated by horizontal lines.

The data become noisier for lighter light quark masses with a fixed heavy quark mass, or for heavier heavy quark mass with fixed light quark mass. As a result, we are not able to extract signals for our lightest light quark $\kappa=0.13816$, except for a few cases when the daughter pion does not have finite spatial momentum. We also note that we carried out simulations for one additional heavy quark mass $aM_0=10.0$. We found, however, that the signal is intolerably noisy, so that we do not use those data in our analysis.

C. Matrix elements

In order to obtain the matrix element $\langle \pi(k_\pi) | V_\mu^{(i)} | B(p_B) \rangle$ from (5.11), we have to eliminate $Z_\pi^L(\mathbf{k}_\pi) Z_B^L(\mathbf{p}_B)$ in the denominator. For this purpose we fit the smeared-smeared and smeared-local two-point functions with a single exponential as in (5.7) and (5.8) for the extraction of $Z_\pi^L(\mathbf{k}_\pi)/\sqrt{E_\pi(\mathbf{k}_\pi)}$, and (5.9) and (5.10) for $Z_B^L(\mathbf{p}_B)/\sqrt{E_B(\mathbf{p}_B)}$. We then obtain a combination

$$\hat{V}_\mu^{(i)}(\mathbf{k}_\pi, \mathbf{p}_B) \equiv \frac{\langle \pi(k_\pi) | V_\mu^{(i)} | B(p_B) \rangle}{\sqrt{E_\pi(\mathbf{k}_\pi) E_B(\mathbf{p}_B)}}. \quad (5.12)$$

Numerical results are listed in Tables V–VIII for each light and heavy quark mass. The first column denotes the momentum configuration as shown in Table IV.

VI. RESULTS FOR THE FORM FACTORS

A. Energy-momentum dispersion relations

In order to extract the form factors from the matrix elements (5.12), we have to determine the meson energy of initial and final states for given spatial momenta. It may be obtained either by assuming a continuum dispersion relation or by actually measuring the meson energy with the given momenta.

For the pion, which is relativistic, the continuum dispersion relation is written as

$$E_\pi(\mathbf{k}_\pi)^2 = M_\pi^2 + \mathbf{k}_\pi^2. \quad (6.1)$$

The measured values of $(aE_\pi(\mathbf{k}_\pi))^2$ for momenta $\mathbf{k}_\pi = (1,0,0)$ and $(1,1,0)$, in unit of $2\pi/La$, are given in Table IX and also plotted in Figure 2 for each light quark mass we calculated. We find a nice agreement with the expectation (6.1). The relation (6.1) may be modified on the lattice due to lattice artifacts; a possible form is given by replacing $a\mathbf{k}_\pi$ with $\sin(a\mathbf{k}_\pi)$, which satisfies the periodic boundary condition. The magnitude of such an effect is not significant, though, since the momentum considered is small enough and the difference between $a\mathbf{k}_\pi$ and $\sin(a\mathbf{k}_\pi)$ is less than 3%.

The dispersion relation for the heavy-light meson is well described by the non-relativistic form

$$E_{\text{bin}}(\mathbf{p}_B) = E_{\text{bin}}(\mathbf{0}) + \frac{\mathbf{p}_B^2}{2M_B}, \quad (6.2)$$

in which the meson mass M_B appears in the kinetic energy term.³ In NRQCD, the heavy-light meson mass is written in terms of the bare mass aM_0 and the binding energy $aE_{\text{bin}}(\mathbf{0})$ as

$$aM_B = Z_m aM_0 - aE_0 + aE_{\text{bin}}(\mathbf{0}), \quad (6.3)$$

where aE_0 is an energy shift and Z_m is a mass renormalization factor. Both factors are calculated at the one-loop level [16,17,19],

$$aE_0 = \alpha_s A, \quad (6.4)$$

$$Z_m = 1 + \alpha_s B, \quad (6.5)$$

and the numerical coefficients A and B are given in Table I of [19]. The heavy-light meson mass evaluated with (6.3) using the V -scheme coupling $\alpha_V(q^*)$ [24] at $q^* = 1/a$ is listed in Table X. Since the one-loop correction partially cancels between $Z_m aM_0$ and aE_0 , the uncertainty due to the choice of q^* is small, *i.e.* at most 3% for $aM_0=1.3$ and even smaller for larger aM_0 .

In Figure 3, a comparison is made of our simulation data with the form of Eq. (6.2) in which the value of M_B evaluated according to Eq. (6.3) is substituted. We find a good agreement except for the data at $\kappa=0.13630$. Even in the worst case, the disagreement does

³ Here we use a capital symbol M_B to represent the generic heavy-light meson mass we deal with on the lattice, whereas keeping m_B to denote the physical B meson mass.

not exceed 1%. Therefore, we employ the dispersion relation (6.2) with the perturbatively estimated meson mass aM_B in the following analysis of the form factors, rather than using the measured binding energy, which has significant statistical errors and complicates our analysis. The same strategy is taken for the pion energy, namely we use the relation (6.1) with the measured value for aM_π .

B. Form factor extraction

The continuum matrix element is obtained from $\hat{V}_\mu^{(i)}(\mathbf{k}_\pi, \mathbf{p}_B)$ defined in (5.12) using the matching formula of the vector current (4.9)–(4.10) as

$$\begin{aligned} \hat{V}_4^{cont}(\mathbf{k}_\pi, \mathbf{p}_B) &= \left(1 + \alpha_s \left[\frac{1}{\pi} \ln(aM_0) + \rho_{V_4}^{(0)} \right] \right) \hat{V}_4^{(0)}(\mathbf{k}_\pi, \mathbf{p}_B) + \alpha_s \rho_{V_4}^{(1)} \hat{V}_4^{(1)}(\mathbf{k}_\pi, \mathbf{p}_B) \\ &\quad + \alpha_s \rho_{V_4}^{(2)} \hat{V}_4^{(2)}(\mathbf{k}_\pi, \mathbf{p}_B), \end{aligned} \quad (6.6)$$

$$\begin{aligned} \hat{V}_k^{cont}(\mathbf{k}_\pi, \mathbf{p}_B) &= \left(1 + \alpha_s \left[\frac{1}{\pi} \ln(aM_0) + \rho_{V_k}^{(0)} \right] \right) \hat{V}_k^{(0)}(\mathbf{k}_\pi, \mathbf{p}_B) + \alpha_s \rho_{V_k}^{(1)} \hat{V}_k^{(1)}(\mathbf{k}_\pi, \mathbf{p}_B) \\ &\quad + \alpha_s \left[\frac{4}{\pi} \ln(aM_0) + \rho_{V_k}^{(2)} \right] \hat{V}_k^{(2)}(\mathbf{k}_\pi, \mathbf{p}_B) + \alpha_s \rho_{V_k}^{(3)} \hat{V}_k^{(3)}(\mathbf{k}_\pi, \mathbf{p}_B) \\ &\quad + \alpha_s \left[-\frac{4}{3\pi} \ln(aM_0) + \rho_{V_k}^{(4)} \right] \hat{V}_k^{(4)}(\mathbf{k}_\pi, \mathbf{p}_B). \end{aligned} \quad (6.7)$$

We use the V -scheme coupling $\alpha_V(q^*)$ for the coupling constant α_s . Since the scale q^* which dominates the lattice one-loop integral is not yet known, we examine the uncertainty in the scale setting by calculating the form factors at $q^* = 1/a$ and at π/a . We use the difference in the results, which is the two-loop effect of $O(\alpha_s^2)$, as an estimate of higher order perturbative errors. The numerical value of the coupling is $\alpha_V(1/a)=0.270$ and $\alpha_V(\pi/a)=0.164$ at $\beta=5.9$ in the quenched approximation.

From the definition of $f_1(v \cdot k_\pi)$ and $f_2(v \cdot k_\pi)$ given in (2.3), we obtain the following formula for the form factors

$$f_1(v \cdot k_\pi) + f_2(v \cdot k_\pi) = \sum_\mu v^\mu \left[\sqrt{\frac{E_\pi(\mathbf{k}_\pi) E_B(\mathbf{p}_B)}{4M_B}} \hat{V}_\mu^{cont}(\mathbf{k}_\pi, \mathbf{p}_B) \right], \quad (6.8)$$

$$f_2(v \cdot k_\pi) \left[1 - \frac{M_\pi^2}{(v \cdot k_\pi)^2} \right] = \sum_\mu \left(v^\mu - \frac{k_\pi^\mu}{(v \cdot k_\pi)} \right) \left[\sqrt{\frac{E_\pi(\mathbf{k}_\pi) E_B(\mathbf{p}_B)}{4M_B}} \hat{V}_\mu^{cont}(\mathbf{k}_\pi, \mathbf{p}_B) \right], \quad (6.9)$$

where $v^\mu = (E_B(\mathbf{p}_B), \mathbf{p}_B)/M_B$ and $k_\pi^\mu = (E_\pi(\mathbf{k}_\pi), \mathbf{k}_\pi)$. By construction, for the initial B meson at rest, $f_1(v \cdot k_\pi) + f_2(v \cdot k_\pi)$ is proportional to the temporal component $\hat{V}_4^{cont}(\mathbf{k}_\pi, \mathbf{p}_B)$, while $f_2(v \cdot k_\pi)$ comes from the spatial component $\hat{V}_k^{cont}(\mathbf{k}_\pi, \mathbf{p}_B)$. Even for a B meson with momentum (1,0,0), the velocity is small ($\mathbf{p}_B/M_B \simeq 0.07$ – 0.2 depending on the heavy quark mass), and the major effect is from the temporal or spatial component for $f_1(v \cdot k_\pi) + f_2(v \cdot k_\pi)$ or for $f_2(v \cdot k_\pi)$, respectively.

An example of the form factors is plotted in Figure 4 for $aM_0=3.0$, which is close to the b quark mass, and $\kappa=0.13630$. The point of smallest $av \cdot k_\pi$ corresponds to the zero recoil configuration, *i.e.* the initial and final particles are at rest so that $av \cdot k_\pi = aM_\pi$. At that point, only the temporal component $\hat{V}_4^{cont}(\mathbf{k}_\pi, \mathbf{p}_B)$ can be measured while the spatial

component vanishes. The momentum configuration $\mathbf{p}_B=(1,0,0)$ and $\mathbf{k}_\pi=(0,0,0)$ gives a very similar $av \cdot k_\pi$, because of large heavy quark mass and small spatial velocity. As a result, the data point almost lies on top of that at zero recoil. We are not able to measure $f_2(v \cdot k_\pi)$ reliably at this point, since the value of the spatial component $\hat{V}_1^{cont}(\mathbf{k}_\pi, \mathbf{p}_B)$ is too small. There are four other momentum configurations (see Table IV), for which both $f_1(v \cdot k_\pi) + f_2(v \cdot k_\pi)$ and $f_2(v \cdot k_\pi)$ are measured. Among them, two momentum configurations sharing the same $\mathbf{k}_\pi=(1,0,0)$ and having different \mathbf{p}_B have almost identical values of $av \cdot k_\pi$ for the same reason as above, and cannot be distinguished from each other in the plot (the middle point of the three filled data points).

From Figure 4 we also see that the effect from choosing $\alpha_V(1/a)$ (circles) or $\alpha_V(\pi/a)$ (squares) is small; it is smaller than the statistical error except for the zero recoil point where the statistical error is minimum. Therefore in the following analysis we use the data with $\alpha_V(1/a)$. In the final results we will include their difference in the systematic error estimation.

C. Heavy quark mass dependence

As we discussed in Section II, the heavy quark scaling is manifest for the form factors $f_1(v \cdot k_\pi)$ and $f_2(v \cdot k_\pi)$. Namely, $f_{1,2}(v \cdot k_\pi)$ behaves as a constant at the leading order of the $1/M$ expansion. Here we examine the heavy quark mass dependence of $f_1(v \cdot k_\pi) + f_2(v \cdot k_\pi)$ and $f_2(v \cdot k_\pi)$ explicitly by comparing the results with different heavy quark masses.

In order to remove the logarithmic dependence on the heavy quark mass that appears from the matching of the vector current between the full QCD and lattice NRQCD (4.9)–(4.10), we define the renormalization group invariant form factors $\Phi_{1+2}(v \cdot k_\pi)$ and $\Phi_2(v \cdot k_\pi)$ as

$$\Phi_{1+2}(v \cdot k_\pi) = \left(\frac{\alpha_s(M_B)}{\alpha_s(m_B)} \right)^{2/\beta_0} [f_1(v \cdot k_\pi) + f_2(v \cdot k_\pi)], \quad (6.10)$$

$$\Phi_2(v \cdot k_\pi) = \left(\frac{\alpha_s(M_B)}{\alpha_s(m_B)} \right)^{2/\beta_0} f_2(v \cdot k_\pi), \quad (6.11)$$

where β_0 denotes the first coefficient of the QCD beta function. We note that M_B is the heavy-light meson mass measured on the lattice for a given aM_0 , while m_B is the physical B meson mass.

Figure 5 shows $\Phi_{1+2}(v \cdot k_\pi)$ and $\Phi_2(v \cdot k_\pi)$ for several values of aM_0 . We find that the $1/M$ correction gives only a small effect in the range of the heavy quark mass we explored which correspond to 2–8 GeV. In fact, there is no significant shift in the magnitude of the form factors by the change of the heavy quark mass. A small effect can be seen in the value of $av \cdot k_\pi$ for a couple of momentum configurations for which $\mathbf{p}_B \cdot \mathbf{k}_\pi \neq 0$. However, it does not seem to change the global shape of the form factors.

The small $1/M$ correction we found is of great phenomenological importance, as it justifies the use of heavy quark symmetry to predict the $B \rightarrow \pi l \nu$ form factors from that of $D \rightarrow \pi l \nu$ and $D \rightarrow K l \nu$ [12]. We discuss this method and possible uncertainties in Section VIII.

D. Light quark mass dependence

In order to obtain the physical form factors we need to extrapolate our result to the physical light (u and d) quark mass. For this purpose we examine the light quark mass dependence of the form factors $f_1(v \cdot k_\pi) + f_2(v \cdot k_\pi)$ and $f_2(v \cdot k_\pi)$ using the data, which covers a range 0.45–0.80 GeV of the pion mass. Unfortunately, the signal is badly contaminated by statistical noise for the lightest data, so that we are not able to extract the form factors except for the zero recoil limit of $f_1(v \cdot k_\pi) + f_2(v \cdot k_\pi)$. For other three κ values, the data is fully available and we mainly use them to see the light quark mass dependence.

Figure 6 shows the measured form factors at four different light quark masses. The heavy quark mass is fixed at $aM_0=2.1$. Since the minimum value of $av \cdot k_\pi$ is aM_π , the range of $av \cdot k_\pi$ where the data is available moves to the left hand side as the light quark mass decreases. On the other hand, change of the value of the form factors $f_1(v \cdot k_\pi) + f_2(v \cdot k_\pi)$ and $f_2(v \cdot k_\pi)$ is not significant if we compare the data for a given momentum configuration. For instance, the values of $a^{1/2}[f_1(v \cdot k_\pi) + f_2(v \cdot k_\pi)]$ stay almost constant around 0.68 over the range $v \cdot k_\pi = 0.27 - 0.49$, which correspond to the lightest and the heaviest data. If we look at the change at fixed $v \cdot k_\pi$, there is an apparent downward shift of $f_1(v \cdot k_\pi) + f_2(v \cdot k_\pi)$. This is due to a negative slope in $av \cdot k_\pi$ in the data at fixed light quark mass. On the other hand, for $f_2(v \cdot k_\pi)$ the light quark mass dependence is less significant, since the data at fixed κ does not seem to have a non-zero slope.

E. Global fit

In order to extract the physical form factors, we have to consider the dependence on three parameters, *i.e.* the inverse heavy meson mass $1/M_B$, the light quark mass m_q and the energy release $v \cdot k_\pi$. The heavy quark effective theory together with the chiral perturbation theory suggests that we can expand the form factors in powers of $1/M_B$ and m_q . On the other hand, there is no theoretical guide in the functional dependence on $v \cdot k_\pi$. Therefore, in fitting the data we use a Taylor expansion around an arbitrary chosen point $v \cdot k_\pi = (v \cdot k_\pi)_0$, which in practice we take in the middle of the measured range. Thus we employ the following form to fit the data,

$$a^{1/2}\Phi_{1+2}(v \cdot k_\pi) = C_{1+2}^{(000)} + \frac{C_{1+2}^{(100)}}{aM_B} + C_{1+2}^{(010)} am_q + \left(C_{1+2}^{(001)} + C_{1+2}^{(011)} am_q \right) [av \cdot k_\pi - (av \cdot k_\pi)_0] + C_{1+2}^{(002)} [av \cdot k_\pi - (av \cdot k_\pi)_0]^2, \quad (6.12)$$

$$a^{1/2}\Phi_2(v \cdot k_\pi) = C_2^{(000)} + \frac{C_2^{(100)}}{aM_B} + C_2^{(010)} am_q + C_2^{(001)} [av \cdot k_\pi - (av \cdot k_\pi)_0], \quad (6.13)$$

where the superscript (ijk) for the coefficient denotes the order of expansion in $1/aM_B$, am_q and $[av \cdot k_\pi - (av \cdot k_\pi)_0]$, in the given order. The fit results for $(av \cdot k_\pi)_0=0.5$ is listed in Table XII.

The choice whether we keep a certain term in (6.12)–(6.13) or drop it is empirical. Our experience in the calculations of the heavy-light decay constant and the B parameters suggests that both the $1/M_B$ and am_q expansions can be safely truncated at the first order. This is consistent with an argument of naive power counting assuming that the relevant

mass scale is around Λ_{QCD} . We find that that is indeed the case also for the $B \rightarrow \pi l \nu$ form factors as we shall discuss in the following.

In (6.12)–(6.13) the $1/M_B$ expansion is truncated at first order, since the $1/M_B$ correction is not significant as discussed in Section VI C so that there is no sensitivity to higher order corrections. Even the first order coefficients $C_{1+2}^{(100)}$ and $C_2^{(100)}$ are consistent with zero within the statistical error. This truncation is also consistent with our NRQCD action, because we do not include the correction of order $1/M_0^2$ or higher in the action (3.2).

The light quark mass dependence of $a^{1/2}\Phi_{1+2}(v \cdot k_\pi)$ is consistent with a linear function if we fix $av \cdot k_\pi$ at $(av \cdot k_\pi)_0=0.5$, for instance. Thus we truncate the expansion in am_q at the first order. We also keep a cross term with the leading $[av \cdot k_\pi - (av \cdot k_\pi)_0]$ correction, but its coefficient $C_{1+2}^{(011)}$ is consistent with zero. For $a^{1/2}\Phi_2(v \cdot k_\pi)$ the light quark mass dependence is not significant as discussed in Section VI D. Although we keep the first order correction to be conservative, its coefficient $C_2^{(010)}$ is almost consistent with zero.

As for the functional dependence of the form factors on $av \cdot k_\pi$, we include the $[av \cdot k_\pi - (av \cdot k_\pi)_0]^2$ term for $a^{1/2}\Phi_{1+2}(v \cdot k_\pi)$, while the second order term is neglected for $a^{1/2}\Phi_2(v \cdot k_\pi)$. The reason is that we find a significant slope in $a^{1/2}\Phi_{1+2}(v \cdot k_\pi)$, so that a higher order term $[av \cdot k_\pi - (av \cdot k_\pi)_0]^2$ is also included for safety. The other form factor $a^{1/2}\Phi_2(v \cdot k_\pi)$ behaves almost like constant, and it is enough to keep the first order term.

While we introduce several terms for which the coefficient is not well determined, *i.e.* consistent with zero, this does not mean our results for the physical form factors have large uncertainty, as far as we use the results for an interpolation in the relevant parameters. For example, the heavy quark mass we simulate covers the b quark mass, so that only an interpolation is required. For the parameter $[av \cdot k_\pi - (av \cdot k_\pi)_0]$, we restrict ourselves to consider the region where the data is available. Therefore, we can obtain the physical form factors in the region $0.67 \text{ GeV} < v \cdot k_\pi < 0.96 \text{ GeV}$ reliably. Outside this region, the fit (6.12)–(6.13) appears to introduce a large uncertainty. For the light quark mass, we have to consider an extrapolation to the physical limit of u and d quarks. This increases our statistical error significantly.

The fit results are shown in Figure 5 (heavy quark mass dependence) and in Figure 6 (light quark mass dependence). In Figure 6 we also plot the limit of physical light quark mass (thick curves), which is obtained by setting am_q to the physical average up and down quark masses in (6.12)–(6.13).

The form factors $f_1(v \cdot k_\pi) + f_2(v \cdot k_\pi)$ and $f_2(v \cdot k_\pi)$ for the physical $B \rightarrow \pi l \nu$ decay is plotted in Figure 7. The region where the lattice data is interpolated in $[av \cdot k_\pi - (av \cdot k_\pi)_0]$ is plotted with symbols. Going outside of that region requires an extrapolation, so that the error shown by dashed curves rapidly grows.

F. Soft pion theorem

In the soft pion limit, *i.e.* m_π and $k_\pi \rightarrow 0$, the following relation (2.10) holds

$$f^0(q_{max}^2) = \frac{2}{\sqrt{M_B}} [f_1(0) + f_2(0)] = \frac{f_B}{f_\pi}. \quad (6.14)$$

It is an important consistency check to see whether one can reproduce this relation in the lattice calculation.

In Figure 8 we plot the result of the fit (6.12) by an open triangle and compare it with the lattice calculation of f_B/f_π (filled triangle) [19]. The data is presented at fixed heavy quark mass $aM_0=3.0$. We should note that the soft pion limit in (6.12) is far from the region where $f_1(v \cdot k_\pi) + f_2(v \cdot k_\pi)$ is obtained by interpolation. Therefore, we expect substantial systematic uncertainty in the fit result. In fact, Figure 7 demonstrates that the extrapolation to $v \cdot k_\pi = 0$ is not yet very stable.

The soft pion limit can also be achieved along a fixed momentum configuration. Namely we may extrapolate the data for each light quark mass at zero recoil. In this case, however, the momentum transfer $v \cdot k_\pi (= M_\pi)$ changes during the extrapolation, so that we have to consider a fit with two terms am_q and aM_π .⁴ Because of the PCAC relation $M_\pi^2 \propto m_q$, it means a quadratic fit in $\sqrt{am_q}$. We plot two extrapolations in Figure 8: a linear form in am_q (dashed line) and a quadratic fit in $\sqrt{am_q}$ (solid curve). Although the effect of the term $\sqrt{am_q}$ seems very small in the data and is only seen at the lightest quark mass, it raises the soft pion limit for the quadratic fit. The result is consistent with the global fit (6.12). Thus we consider that the disagreement of $f^0(q_{max}^2)$ with f_B/f_π , which seemed to be a serious problem by only looking at the naive linear extrapolation with only data at zero recoil, is in fact more of a problem in the subtle chiral extrapolation or in the model uncertainty of momentum extrapolation.

The UKQCD [26,25] and APE [7,27] collaborations found in their study with the relativistic heavy quark action that the soft pion relation (6.14) is satisfied. It should be noted, however, that their method of chiral extrapolation corresponds to our “global fit” method, and the measured kinematical region is far from the soft pion limit. Therefore the result in the soft pion limit should depend on how the extrapolation is made. They employed a pole-like model [28] for their fit function. Thus their results in the soft pion limit contain some uncertainty which is not well controlled just as ours, although the results in the kinematical region obtained by interpolating the lattice data do not suffer from such uncertainties.

Judging from the size of the uncertainties it is too early to consider the deviation from the soft pion relation as a serious problem. This problem can be studied with much statistically significant data with larger number of momentum points and light quark masses so that the extrapolation in $v \cdot k_\pi$ towards the soft pion limit becomes more stable, which is still beyond the scope of this paper.

G. Pole dominance

In the soft pion limit, the heavy meson effective lagrangian predicts the B^* pole dominance (2.11), that is

$$\lim_{v \cdot k_\pi \rightarrow 0} f_2(v \cdot k_\pi) = g \frac{f_{B^*} \sqrt{m_{B^*}}}{2f_\pi} \frac{v \cdot k_\pi}{v \cdot k_\pi + \Delta_B}. \quad (6.15)$$

⁴ As discussed in [25], one should include a term which is linear in aM_π when $v \cdot k_\pi$ (or q^2 in the relativistic form) varies during the extrapolation of form factors. The fit becomes more stable if one first interpolates to a fixed $v \cdot k_\pi$ (or q^2), and then extrapolate in am_q . Our strategy to employ the global fit (6.12)–(6.13) is equivalent to this method.

Since the hyperfine splitting $\Delta_B \equiv M_{B^*} - M_B$ is much smaller than the momentum transfer $v \cdot k_\pi$ we measure, we can approximate its functional form by a constant in our data region. Our data support the constant behavior and give $g(f_{B^*} \sqrt{am_{B^*}}/2f_\pi) = 0.35(18)$ which reduces to $g = 0.30(16)$. This agrees with the phenomenological value extracted from $D^* \rightarrow D\pi$ decay 0.27(6) [29], and also with the recent lattice calculation $g = 0.42(4)(8)$ [30], which is obtained for the static heavy quark. The agreement suggests that the $1/M$ correction is small for the form factors.

H. Systematic Errors

We now discuss possible sources of systematic errors and their estimates. Since the statistical error, the discretization error of $O(a^2)$, the perturbative error of $O(\alpha_s^2)$, and the chiral extrapolation error are large, we only consider these dominant sources of errors and neglect other subleading errors such as $O(\alpha_s^2/(aM))$, $O(\alpha_s^2 a \Lambda_{QCD})$, $O(\alpha_s \Lambda_{QCD}/M)$ and so on.

The size of the two-loop order correction is only known by explicit computation, which is beyond the scope of this paper. Instead, we estimate the size of the perturbative error of $O(\alpha_s^2)$ as half of the difference of values for $q^* = \pi/a$ and $1/a$. The typical sizes are 1.5% for $f_1(v \cdot k_\pi) + f_2(v \cdot k_\pi)$ and 3.5% for $f_2(v \cdot k_\pi)$. The reason for the error for $f_2(v \cdot k_\pi)$ being larger is that the one-loop renormalization coefficient for heavy-light vector current is larger for the spatial component than for the temporal one and that the matrix element of the spatial component gives larger contributions to $f_2(v \cdot k_\pi)$ in the small recoil region.

The discretization errors of $O(a^2 \Lambda_{QCD}^2)$ and of $O(a^2 \mathbf{k}_\pi^2)$ are also important. The former error is common to most lattice simulations using the $O(a)$ -improved actions, and through an order counting we estimate it to be 3% at $\beta = 5.9$ assuming that the typical momentum scale Λ_{QCD} is around 300 MeV. The latter is specific to the present work since the error due to nonzero recoil momenta appears only in the study of form factors. As the pion momentum treated in our calculation is at most $2\pi/L$ ($L=16$) in the lattice unit, we estimate this error to be about 16% using the order estimation.

The error in the chiral extrapolation is another major source of the systematic error. Since we have data at only three κ values except for the zero recoil point, it is not practical to test different functional forms in m_q for the chiral extrapolation. We instead estimate the corresponding error in the form factors by taking the square of the difference between the result of the chiral limit and that of the lightest κ . This gives 10% for $f_1(v \cdot k_\pi) + f_2(v \cdot k_\pi)$ and 1% for $f_2(v \cdot k_\pi)$.

The total error is estimated by adding these errors in quadrature together with the statistical error. In Figure 9 the form factors $f_1(v \cdot k_\pi) + f_2(v \cdot k_\pi)$ and $f_2(v \cdot k_\pi)$ are plotted with the estimated systematic uncertainties. Numerical results are listed in Table XIII.

VII. COMPARISON WITH OTHER CALCULATIONS

A. $f_1(v \cdot k_\pi)$ and $f_2(v \cdot k_\pi)$

The Fermilab group calculated the form factors at the b quark mass using the non-relativistic interpretation of the relativistic lattice action [11]. A comparison is made with our results for the HQET form factors $f_1(v \cdot k_\pi) + f_2(v \cdot k_\pi)$ and $f_2(v \cdot k_\pi)$ at the same β value employed, $\beta=5.9$, in Figure 10. We find a reasonable agreement for $f_2(v \cdot k_\pi)$, but for $f_1(v \cdot k_\pi) + f_2(v \cdot k_\pi)$ our data seem substantially lower.

Since both NRQCD and Fermilab action are the two variants of the nonrelativistic effective action, there should be no fundamental difference in the result. There can be, however, two possible reasons for the disagreement. One is the difference in the renormalization factor. The other is the difference in various systematic errors which arise from the choice of parameters such as the lattice size, smearing methods, fitting procedures and so on.

In order to see the reason of the disagreement, we plot the form factors at a fixed momentum configuration $a\mathbf{p}_B = (0, 0, 0)$ and $a\mathbf{k}_\pi = (1, 0, 0)$ as a function of the light quark mass in Figure 11. While we find a good agreement for $f_2(v \cdot k_\pi)$, our results for $f_1(v \cdot k_\pi) + f_2(v \cdot k_\pi)$ is significantly lower than the Fermilab data. Furthermore, in the fit of the form (6.12) the chiral limit of our data is lower than the data at finite am_q as shown in the plot, in contrast to the Fermilab data, for which the chiral limit becomes even higher due to a positive curvature.

We note that the renormalization of the vector current is made using the non-perturbative Z factors of heavy-heavy and light-light current in the Fermilab analysis [11]. A correction is then made perturbatively for the heavy-light current. Since our results are obtained with an entirely perturbative matching, systematic errors may enter differently. The effect of such a ‘partial’ non-perturbative renormalization for the NRQCD action is an issue of future investigation.

We should also note that in Figure 11 the statistical error in our calculation seems much larger than that in the Fermilab data, despite much larger statistics in our calculation. We suspect that the main reason for the large statistical error in our data is a larger temporal extent of our lattice $N_T=48$ compared to $N_T=32$ in the Fermilab work. The large temporal size and the large distance between t_π and t_B in our simulation renders the extraction of the ground state contribution very convincing as shown in Figure 1, which seems much better than the equivalent plot in [11], but at the same time the statistical noise exponentially grows as the heavy-light meson evolves in the temporal direction [31,32].

B. $f^+(q^2)$ and $f^0(q^2)$

A comparison of the form factors in the conventional definition $f^+(q^2)$ and $f^0(q^2)$ is made in Figure 12. Results from recent lattice calculations by APE [7], UKQCD [6] and Fermilab [11] are shown in the plot together with our data.

We find that all data is consistent with each other for $f^+(q^2)$, while our result is somewhat lower for $f^0(q^2)$. Since $f^0(q^2)$ is proportional to $f_1(v \cdot k_\pi) + f_2(v \cdot k_\pi)$ up to a small correction of $O(v \cdot k_\pi/m_B)$, the disagreement with the Fermilab result is the same one as we discussed in the previous subsection.

The results of other two groups, APE and UKQCD, are lower than the Fermilab result to but still higher than ours. We note that in their approach an extrapolation

in $1/M_P$ is necessary to predict the B meson form factor from the simulation results for lighter heavy quarks. Figure 13 shows such an extrapolation. The magnitude of $\Phi_0(\equiv (\alpha_s(M_P)/\alpha_s(M_B))^{-2/11} f^0 \sqrt{M_P})$ in their results agrees with ours, but the APE results show a negative slope in contrast to a flat $1/M$ dependence of our data, leading to the APE value at the physical point considerably higher than ours. In the relativistic approach, the discretization error may be magnified toward heavier quarks, since the discretization error scales as a power of aM . Therefore, the dependence on the heavy quark mass can be badly distorted. Furthermore, the heavy quark expansion becomes questionable for lighter heavy quarks, and the extrapolation with a linear or quadratic function in $1/M_P$ may not be sufficient. Such effects are difficult to incorporate in the extrapolation, and the systematic error can be underestimated.

VIII. PHENOMENOLOGICAL IMPLICATIONS

A. Differential decay rate

The differential decay rate of the semileptonic $B^0 \rightarrow \pi^- l^+ \nu_l$ decay is proportional to the form factor $f^+(q^2)$ squared,

$$\frac{1}{|V_{ub}|^2} \frac{d\Gamma}{dq^2} = \frac{G_F^2}{24\pi^3} |\mathbf{k}_\pi|^3 |f^+(q^2)|^2. \quad (8.1)$$

Therefore, if a reliable calculation of the form factor is available from lattice QCD, the experimental data can be used to extract the CKM element $|V_{ub}|$. Our result for the differential decay rate divided by $|V_{ub}|^2$ is listed in Table XIII and shown in Figure 14.

The momentum configuration where data is available is limited to a large q^2 region, $18 \text{ GeV}^2 < q^2 < 21 \text{ GeV}^2$, which corresponds to small recoil momenta. In the region above 21 GeV^2 there is no data point because of large pion mass in the lattice calculations. However, the pole dominance near zero recoil region (2.11) and (2.12), which is confirmed in part by our lattice calculations, should become even better approximation in that region. Therefore, the theoretical uncertainty is under control in that large q^2 region. A strategy to determine $|V_{ub}|$ is, then, to measure the decay rate in the large q^2 region, $q^2 > 18 \text{ GeV}^2$, and to use the lattice result

$$\frac{G_F^2}{24\pi^3} \int_{18\text{GeV}^2}^{q_{max}^2} dq^2 |\mathbf{k}_\pi|^3 |f^+(q^2)|^2 = 1.18 \pm 0.37 \pm 0.08 \pm 0.31 \text{ psec}^{-1} \quad (8.2)$$

The first error is statistical, the second is perturbative and the last error is the error from discretization and chiral extrapolation.

B. $D \rightarrow \pi l \nu$ and $D \rightarrow K l \nu$

As we found in Section VIC, the $1/M$ correction to the HQET form factors $f_1(v \cdot k_\pi)$ and $f_2(v \cdot k_\pi)$ is small. Although our data is only available for large heavy quark mass $M > 3.2 \text{ GeV}$ and the charm quark mass is not covered, the result suggests that the semileptonic

decays of D mesons, $D \rightarrow \pi l \nu$ and $D \rightarrow K l \nu$, may be used to constrain the form factors, as proposed by Burdman *et al.* [12].

The idea of [12] is to consider a ratio of the differential decay rates of $B \rightarrow \pi l \nu$ and $D \rightarrow \pi l \nu$ at a fixed recoil energy $v \cdot k_\pi$, then the heavy quark symmetry tells us that the ratio is unity at the leading order, and the ratio of CKM elements $|V_{ub}/V_{cd}|$ may be extracted without model dependence. The method is, however, not so useful unless the size of $1/M$ (and higher order) corrections is reliably estimated. The lattice calculation could be used to evaluate them, as we attempt in this work.

In the lattice calculation, the bulk of systematic errors, especially uncertainty in the perturbative renormalization, is canceled in the ratio of form factors with different heavy quark mass. This idea was extensively used by the Fermilab group [33,34] in the lattice study of heavy-to-heavy decay, namely $B \rightarrow D^{(*)} l \nu$, in which the heavy quark symmetry predicts a stronger constraint and the form factor is even normalized in the zero recoil limit up to a correction of $O(1/M^2)$ that can be calculated on the lattice. The Fermilab group also considered the ratio for the heavy-to-light decay [11]. They calculated the form factors at b and c quark masses, and found a small but significant mass dependence in the HQET form factors, which might conflict with our findings. It is, therefore, important to extend our work toward lighter heavy quarks in order to investigate how the form factors are modified by the $1/M$ corrections. We also note that for this purpose the non-relativistic interpretation of the relativistic lattice action [10] employed in [11] is best suited, because lighter heavy quark can be treated without large systematic errors.

IX. CONCLUSIONS

In this paper, we calculated the form factors and the differential decay rate for $B \rightarrow \pi l \nu$ on the quenched lattice using the NRQCD action. In the HQET form factors $f_1(v \cdot k_\pi)$ and $f_2(v \cdot k_\pi)$, the heavy quark mass dependence appears only in the form of the $1/M$ expansion. From calculations at several different heavy quark masses we found that the $1/M$ correction is not significant for these form factors. We found that the B^* pole contribution dominates $f^+(q^2)$ for small pion recoil energy. We also showed that the extrapolation to the soft pion limit suffers from large systematic errors, so that the discrepancies between $f^0(q_{max}^2)$ and f_B/f_π in the soft pion relation, as seen, in the present simulation is not a serious problem.

In order to avoid the model dependence, we did not assumed any particular functional form for the form factors. Instead, we carried out an interpolation in the region where our data are available. Although the accessible q^2 region is rather limited, the prediction from chiral effective lagrangian may be used to extend the prediction toward q_{max}^2 , and we obtained a partially integrated differential decay rate in the region $18 \text{ GeV} < q^2 < q_{max}^2$. We obtained $\frac{G_F^2}{24\pi^3} \int_{18\text{GeV}^2}^{q_{max}^2} dq^2 |\mathbf{k}_\pi|^3 |f^+(q^2)|^2 = 1.18 \pm 0.37 \pm 0.08 \pm 0.31 \text{psec}^{-1}$ where the first error is statistical error the second is the error from perturbative calculation and the third is the systematic error from the discretization and chiral extrapolation.

The discretization error of $O(a^2)$ and the perturbative error are sizable. The first error can be reduced by performing simulation at several different lattice spacings and/or using different lattice actions. The reduction of the second error is more demanding. We need a non-perturbative renormalization to remove it. Another important source of uncertainty,

which we did not include, is the quenched approximation, whose effect can be estimated only with simulations including dynamical quarks. We are planning future studies in these directions.

ACKNOWLEDGMENT

We thank Andreas Kronfeld for useful discussion and for providing us with their numerical data for comparison. This work is supported by the Supercomputer Project No.66 (FY2001) of High Energy Accelerator Research Organization (KEK), and also in part by the Grants-in-Aid of the Ministry of Education (Nos. 10640246, 11640294, 12014202, 12640253, 12640279, 12740133, 13640260 and 13740169). K.-I.I. and N.Y. are supported by the JSPS Research Fellowship.

REFERENCES

- [1] J.P. Alexander *et al.* (CLEO collaboration), Phys. Rev. Lett. **77**, 5000 (1996).
- [2] B.H. Behrens *et al.* (CLEO collaboration), Phys. Rev. **D 61**, 052001 (2000).
- [3] C. Bernard, presented at the 18th International Symposium on Lattice Field Theory (Lattice 2000), Bangalore, India, August 2000, hep-lat/0011064.
- [4] S. Hashimoto, in proceedings of the 17th International Symposium on Lattice Field Theory (Lattice'99), Pisa, Italy, June-July 1999, Nucl. Phys. (Proc. Suppl.) **83-84** (2000) 3.
- [5] J.M. Flynn and C.T. Sachrajda, in "Heavy Flavours II", ed. by A.J. Buras and M. Lindner (World Scientific, Singapore, 1998).
- [6] UKQCD collaboration (K.C. Bowler *et al.*), Phys. Lett. **B486** (2000) 111.
- [7] A. Abada, D. Becirevic, Ph. Boucaud, J.P. Leroy, V. Lubicz, F. Mescia, hep-lat/0011065
- [8] B.A. Thacker and G.P. Lepage, Phys. Rev. **D43** (1991) 196; G.P. Lepage, L. Magnea, C. Nakhleh, U. Magnea, and K. Hornbostel, Phys. Rev. **D46** (1992) 4052.
- [9] S. Hashimoto, K.-I. Ishikawa, H. Matsufuru, T. Onogi, and N. Yamada, Phys. Rev. **D58**, 014502 (1998).
- [10] A.X. El-Khadra, A.S. Kronfeld and P.B. Mackenzie, Phys. Rev. **D55**, 3933 (1997).
- [11] A.X. El-Khadra, A.S. Kronfeld, P.B. Mackenzie, S.M. Ryan and J.N. Simone, hep-ph/0101023.
- [12] G. Burdman, Z. Ligeti, M. Neubert, and Y. Nir, Phys. Rev. **D49** (1994) 2331,
- [13] For a review, see, R. Casalbuoni, A. Deandrea, N. Di Bartolomeo, R. Gatto, F. Feruglio and G. Nardulli, Phys. Rept. **281** (1997) 145.
- [14] S. Hashimoto and H. Matsufuru, Phys. Rev. **D54** (1996) 4578.
- [15] J.H. Sloan, Nucl. Phys. (Proc. Suppl.) **63** (1998) 365.
- [16] C.T.H. Davies and B.A. Thacker, Phys. Rev. **D45** (1992) 915.
- [17] C.J. Morningstar Phys. Rev. **D48** (1993) 2265.
- [18] S. Hashimoto, K.-I. Ishikawa, H. Matsufuru, T. Onogi, S. Tominaga and N. Yamada, Phys. Rev. **D60**, 094503 (1999).
- [19] JLQCD Collaboration (K.-I. Ishikawa *et al.*), Phys. Rev. **D61**, 074501 (2000).
- [20] S. Hashimoto, K.-I. Ishikawa, T. Onogi, M. Sakamoto, N. Tsutsui and N. Yamada, Phys. Rev. **D62**, 114502 (2000).
- [21] C.J. Morningstar and J. Shigemitsu, Phys. Rev. **D57** (1998) 6741.
- [22] C.J. Morningstar and J. Shigemitsu, Phys. Rev. **D59**, 094504 (1999).
- [23] B. Sheikholeslami and R. Wohlert, Nucl. Phys. **B259** (1985) 572.
- [24] G.P. Lepage and P.B. Mackenzie, Phys. Rev. **D48** (1993) 2250.
- [25] UKQCD collaboration (C.M. Maynard *et al.*), presented at the 18th International Symposium on Lattice Field Theory (Lattice 2000), Bangalore, India, August 2000, hep-lat/0010016.
- [26] UKQCD collaboration (V. Lesk *et al.*), in proceedings of the 17th International Symposium on Lattice Field Theory (Lattice'99), Pisa, Italy, June-July 1999, Nucl. Phys. (Proc. Suppl.) **83-84** (2000) 313; UKQCD collaboration (C.M. Maynard *et al.*), in proceedings of the 17th International Symposium on Lattice Field Theory (Lattice'99), Pisa, Italy, June-July 1999, Nucl. Phys. (Proc. Suppl.) **83-84** (2000) 322.
- [27] D. Becirevic, presented at the 18th International Symposium on Lattice Field Theory (Lattice 2000), Bangalore, India, August 2000, hep-lat/0011075.

- [28] D. Becirevic and A. Kaidalov, Phys. Lett. **B478** (2000) 417.
- [29] I.W. Stewart, Nucl. Phys. **B529** (1998) 62.
- [30] UKQCD collaboration (G.M. de Divitiis, L. Del Debbio, M. Di Pierro, J.M. Flynn, C. Michael and J. Peisa), JHEP **10** (1998) 010.
- [31] G.P. Lepage, Nucl. Phys. B (Proc. Suppl.) **26** (1992) 45.
- [32] S. Hashimoto, Phys. Rev. **D50** (1994) 4639.
- [33] S. Hashimoto, A.X. El-Khadra, A.S. Kronfeld, P.B. Mackenzie, S.M. Ryan, and J.N. Simone, Phys. Rev. **D61**, 014502 (2000).
- [34] J.N. Simone, S. Hashimoto, A.X. El-Khadra, A.S. Kronfeld, P.B. Mackenzie, S.M. Ryan, presented at the 17th International Symposium on Lattice Field Theory (LATTICE 99), Pisa, Italy, 29 Jun - 3 Jul 1999, Nucl. Phys. (Proc. Suppl.) **83-84** (2000) 334.

TABLES

aM_0	n	$\rho_{V_4}^{(0)}$	$\rho_{V_4}^{(1)}$	$\rho_{V_4}^{(2)}$
10.0	2	-0.562	-0.572	-0.421
5.0	2	-0.554	-0.571	0.205
3.0	2	-0.540	-0.582	0.446
2.1	3	-0.529	-0.604	0.559
1.3	3	-0.509	-0.629	0.657

TABLE I. Renormalization constants for V_4 .

aM_0	n	$\rho_{V_k}^{(0)}$	$\rho_{V_k}^{(1)}$	$\rho_{V_k}^{(2)}$	$\rho_{V_k}^{(3)}$	$\rho_{V_k}^{(4)}$
10.0	2	-1.250	0.366	13.705	0.983	1.047
5.0	2	-1.087	0.232	4.678	0.881	0.977
3.0	2	-0.915	0.091	1.605	0.774	0.893
2.1	3	-0.772	-0.049	0.594	0.690	0.812
1.3	3	-0.546	-0.235	0.188	0.587	0.668

TABLE II. Renormalization constants for V_k .

aM_0	a_h	b_h
10.0	0.16	1.50
5.0	0.28	1.12
3.0	0.29	1.07
2.1	0.30	1.06
1.3	0.31	1.06

TABLE III. Smearing parameters for the heavy-light meson.

id.	\boldsymbol{p}_B	\boldsymbol{k}_π	\boldsymbol{q}
p000.q000	(0,0,0)	(0,0,0)	(0,0,0)
p100.q100	(1,0,0)	(0,0,0)	(1,0,0)
p100.q000	(1,0,0)	(1,0,0)	(0,0,0)
p100.q110	(1,0,0)	(0,-1,0)	(1,1,0)
p000.q100	(0,0,0)	(-1,0,0)	(1,0,0)
p100.q200	(1,0,0)	(-1,0,0)	(2,0,0)

TABLE IV. List of momenta for which the three-point correlator is measured. Three-momentum is given in the unit of $2\pi/La$. 'id.' will be used in the tables of numerical results.

$aM_0=5.0$								
id.	$\hat{V}_4^{(0)}$	$\hat{V}_4^{(1)}$	$\hat{V}_4^{(2)}$	$\hat{V}_1^{(0)}$	$\hat{V}_1^{(1)}$	$\hat{V}_1^{(2)}$	$\hat{V}_1^{(3)}$	$\hat{V}_1^{(4)}$
p000.q000	2.059(44)	0.1874(53)	-0.1874(53)					
p100.q100	2.052(52)	0.2304(72)	-0.1862(60)	0.010(10)	-0.660(17)	0.001(3)	-0.713(18)	-0.053(4)
p100.q000	1.79(17)	-0.023(28)	0.023(28)	0.876(90)	-0.496(53)	0.013(20)	-0.241(26)	0.241(26)
p100.q110	1.645(64)	0.272(15)	0.0602(86)	-0.740(30)	-0.121(26)	0.004(5)	-0.358(20)	-0.266(10)
p000.q100	1.554(56)	0.216(13)	0.0603(97)	-0.751(29)	-0.063(23)	0.011(7)	-0.321(19)	-0.268(11)
p100.q200	1.34(11)	0.487(43)	0.073(20)	-0.697(62)	-0.547(70)	0.042(16)	-0.765(71)	-0.263(25)
$aM_0=3.0$								
id.	$\hat{V}_4^{(0)}$	$\hat{V}_4^{(1)}$	$\hat{V}_4^{(2)}$	$\hat{V}_1^{(0)}$	$\hat{V}_1^{(1)}$	$\hat{V}_1^{(2)}$	$\hat{V}_1^{(3)}$	$\hat{V}_1^{(4)}$
p000.q000	2.087(33)	0.217(41)	-0.2173(41)					
p100.q100	2.066(39)	0.2802(60)	-0.2126(47)	0.031(8)	-0.632(12)	0.016(2)	-0.697(13)	-0.081(3)
p100.q000	1.81(16)	0.008(23)	-0.008(23)	0.877(80)	-0.416(44)	0.003(16)	-0.207(22)	0.207(22)
p100.q110	1.621(57)	0.302(13)	0.0426(66)	-0.704(26)	-0.152(22)	0.034(4)	-0.351(17)	-0.274(9)
p000.q100	1.547(50)	0.231(11)	0.0390(73)	-0.710(25)	-0.096(18)	0.0393(53)	-0.325(16)	-0.268(9)
p100.q200	1.343(94)	0.495(34)	0.073(15)	-0.627(46)	-0.544(53)	0.076(13)	-0.762(57)	-0.296(20)
$aM_0=2.1$								
id.	$\hat{V}_4^{(0)}$	$\hat{V}_4^{(1)}$	$\hat{V}_4^{(2)}$	$\hat{V}_1^{(0)}$	$\hat{V}_1^{(1)}$	$\hat{V}_1^{(2)}$	$\hat{V}_1^{(3)}$	$\hat{V}_1^{(4)}$
p000.q000	2.108(30)	0.2552(41)	-0.2552(41)					
p100.q100	2.072(35)	0.3354(61)	-0.2469(46)	0.057(7)	-0.606(10)	0.030(2)	-0.680(11)	-0.105(3)
p100.q000	1.85(16)	0.050(22)	-0.050(22)	0.898(73)	-0.347(39)	-0.008(14)	-0.178(19)	0.178(19)
p100.q110	1.607(51)	0.341(12)	0.0172(58)	-0.683(23)	-0.184(18)	0.060(4)	-0.350(15)	-0.278(8)
p000.q100	1.555(47)	0.254(10)	0.0129(65)	-0.686(22)	-0.130(15)	0.064(5)	-0.333(14)	-0.268(8)
p100.q200	1.321(86)	0.504(32)	0.067(15)	-0.556(41)	-0.551(48)	0.117(16)	-0.749(51)	-0.315(19)
$aM_0=1.3$								
id.	$\hat{V}_4^{(0)}$	$\hat{V}_4^{(1)}$	$\hat{V}_4^{(2)}$	$\hat{V}_1^{(0)}$	$\hat{V}_1^{(1)}$	$\hat{V}_1^{(2)}$	$\hat{V}_1^{(3)}$	$\hat{V}_1^{(4)}$
p000.q000	2.140(25)	0.3278(40)	-0.3278(40)					
p100.q100	2.066(34)	0.4323(74)	-0.3087(54)	0.103(6)	-0.556(10)	0.057(2)	-0.644(10)	-0.146(3)
p100.q000	1.94(16)	0.136(24)	-0.136(24)	0.943(66)	-0.229(34)	-0.030(12)	-0.130(16)	0.130(16)
p100.q110	1.519(45)	0.399(14)	-0.0227(63)	-0.636(23)	-0.234(16)	0.103(5)	-0.338(13)	-0.269(8)
p000.q100	1.581(45)	0.304(10)	-0.0361(63)	-0.655(19)	-0.189(14)	0.110(5)	-0.348(13)	-0.269(7)
p100.q200	1.278(71)	0.551(30)	0.049(11)	-0.478(31)	-0.564(39)	0.180(14)	-0.733(41)	-0.349(17)

TABLE V. Matrix elements $\hat{V}_\mu^{(i)}$ at $\kappa=0.13630$. The first column represents the momentum configuration as defined in Table IV.

$aM_0=5.0$								
id.	$\hat{V}_4^{(0)}$	$\hat{V}_4^{(1)}$	$\hat{V}_4^{(2)}$	$\hat{V}_1^{(0)}$	$\hat{V}_1^{(1)}$	$\hat{V}_1^{(2)}$	$\hat{V}_1^{(3)}$	$\hat{V}_1^{(4)}$
p000.q000	2.222(61)	0.2754(88)	-0.2754(88)					
p100.q100	2.211(70)	0.326(11)	-0.2756(99)	-0.005(13)	-0.708(23)	-0.009(4)	-0.772(24)	-0.056(5)
p100.q000	1.76(30)	0.051(40)	-0.051(40)	1.11(15)	-0.523(82)	0.071(28)	-0.224(41)	0.224(41)
p100.q110	1.71(11)	0.338(31)	0.036(15)	-0.843(59)	-0.126(46)	-0.056(10)	-0.408(36)	-0.243(19)
p000.q100	1.50(10)	0.262(26)	0.038(17)	-0.826(56)	-0.037(41)	-0.037(13)	-0.322(34)	-0.249(20)
p100.q200	1.31(19)	0.556(78)	0.074(30)	-0.81(11)	-0.53(12)	-0.008(26)	-0.77(12)	-0.229(40)
$aM_0=3.0$								
id.	$\hat{V}_4^{(0)}$	$\hat{V}_4^{(1)}$	$\hat{V}_4^{(2)}$	$\hat{V}_1^{(0)}$	$\hat{V}_1^{(1)}$	$\hat{V}_1^{(2)}$	$\hat{V}_1^{(3)}$	$\hat{V}_1^{(4)}$
p000.q000	2.242(48)	0.3050(72)	-0.3050(72)					
p100.q100	2.217(54)	0.375(10)	-0.3003(80)	0.019(11)	-0.679(17)	0.009(3)	-0.755(18)	-0.085(4)
p100.q000	1.81(27)	0.063(31)	-0.063(31)	1.06(12)	-0.408(65)	0.058(19)	-0.175(32)	0.175(32)
p100.q110	1.667(97)	0.362(27)	0.020(12)	-0.789(50)	-0.151(38)	-0.020(7)	-0.390(30)	-0.256(15)
p000.q100	1.485(89)	0.268(21)	0.020(13)	-0.771(47)	-0.076(32)	-0.004(10)	-0.326(29)	-0.247(15)
p100.q200	1.32(15)	0.564(59)	0.062(21)	-0.726(81)	-0.519(87)	0.034(18)	-0.770(93)	-0.285(30)
$aM_0=2.1$								
id.	$\hat{V}_4^{(0)}$	$\hat{V}_4^{(1)}$	$\hat{V}_4^{(2)}$	$\hat{V}_1^{(0)}$	$\hat{V}_1^{(1)}$	$\hat{V}_1^{(2)}$	$\hat{V}_1^{(3)}$	$\hat{V}_1^{(4)}$
p000.q000	2.254(42)	0.3434(67)	-0.3434(67)					
p100.q100	2.214(50)	0.431(10)	-0.3345(81)	0.050(10)	-0.650(15)	0.024(2)	-0.737(16)	-0.111(4)
p100.q000	1.85(25)	0.092(30)	-0.092(30)	1.05(11)	-0.330(56)	0.046(16)	-0.141(27)	0.141(27)
p100.q110	1.634(86)	0.399(25)	-0.005(10)	-0.765(43)	-0.183(32)	0.013(6)	-0.382(27)	-0.263(13)
p000.q100	1.495(83)	0.287(20)	-0.003(11)	-0.743(42)	-0.115(28)	0.024(8)	-0.337(26)	-0.247(13)
p100.q200	1.31(12)	0.590(51)	0.055(17)	-0.679(61)	-0.539(71)	0.076(15)	-0.777(78)	-0.314(26)
$aM_0=1.3$								
id.	$\hat{V}_4^{(0)}$	$\hat{V}_4^{(1)}$	$\hat{V}_4^{(2)}$	$\hat{V}_1^{(0)}$	$\hat{V}_1^{(1)}$	$\hat{V}_1^{(2)}$	$\hat{V}_1^{(3)}$	$\hat{V}_1^{(4)}$
p000.q000	2.276(35)	0.4170(66)	-0.4170(66)					
p100.q100	2.193(43)	0.527(10)	-0.3956(80)	0.1038(80)	-0.595(12)	0.0531(20)	-0.697(13)	-0.1557(37)
p100.q000	1.91(23)	0.146(35)	-0.146(35)	1.02(10)	-0.215(47)	0.019(17)	-0.098(23)	0.098(23)
p100.q110	1.486(72)	0.443(25)	-0.041(11)	-0.701(40)	-0.225(27)	0.0644(74)	-0.352(23)	-0.254(11)
p000.q100	1.529(76)	0.332(19)	-0.049(11)	-0.711(34)	-0.182(23)	0.0754(82)	-0.356(22)	-0.250(12)
p100.q200	1.28(10)	0.620(47)	0.037(14)	-0.575(45)	-0.559(56)	0.149(15)	-0.765(62)	-0.355(23)

TABLE VI. Matrix elements $\hat{V}_\mu^{(i)}$ at $\kappa=0.13711$.

$aM_0=5.0$								
id.	$\hat{V}_4^{(0)}$	$\hat{V}_4^{(1)}$	$\hat{V}_4^{(2)}$	$\hat{V}_1^{(0)}$	$\hat{V}_1^{(1)}$	$\hat{V}_1^{(2)}$	$\hat{V}_1^{(3)}$	$\hat{V}_1^{(4)}$
p000.q000	2.433(92)	0.382(15)	-0.382(15)					
p100.q100	2.42(10)	0.448(21)	-0.385(17)	-0.031(21)	-0.771(34)	-0.020(60)	-0.850(37)	-0.059(8)
p100.q000	1.75(55)	0.118(75)	-0.118(75)	1.47(31)	-0.57(15)	0.170(62)	-0.197(77)	0.197(77)
p100.q110	1.74(19)	0.390(63)	0.019(29)	-0.94(11)	-0.130(85)	-0.120(23)	-0.461(65)	-0.203(35)
p000.q100	1.33(17)	0.292(50)	0.014(32)	-0.85(11)	0.007(75)	-0.081(28)	-0.288(63)	-0.224(36)
p100.q200	1.36(33)	0.70(16)	0.089(53)	-1.06(24)	-0.55(22)	-0.061(53)	-0.83(21)	-0.216(74)
$aM_0=3.0$								
id.	$\hat{V}_4^{(0)}$	$\hat{V}_4^{(1)}$	$\hat{V}_4^{(2)}$	$\hat{V}_1^{(0)}$	$\hat{V}_1^{(1)}$	$\hat{V}_1^{(2)}$	$\hat{V}_1^{(3)}$	$\hat{V}_1^{(4)}$
p000.q000	2.439(71)	0.411(12)	-0.411(12)					
p100.q100	2.413(78)	0.494(17)	-0.406(13)	-0.001(17)	-0.738(24)	-0.000(4)	-0.830(27)	-0.091(6)
p100.q000	1.76(50)	0.111(60)	-0.111(60)	1.38(25)	-0.40(11)	0.145(45)	-0.127(60)	0.127(60)
p100.q110	1.69(16)	0.407(53)	0.003(22)	-0.864(96)	-0.142(68)	-0.076(16)	-0.430(54)	-0.230(28)
p000.q100	1.31(15)	0.283(42)	0.004(24)	-0.785(91)	-0.043(58)	-0.038(19)	-0.294(53)	-0.218(27)
p100.q200	1.37(26)	0.70(12)	0.057(38)	-0.92(16)	-0.55(15)	-0.006(34)	-0.83(16)	-0.284(56)
$aM_0=2.1$								
id.	$\hat{V}_4^{(0)}$	$\hat{V}_4^{(1)}$	$\hat{V}_4^{(2)}$	$\hat{V}_1^{(0)}$	$\hat{V}_1^{(1)}$	$\hat{V}_1^{(2)}$	$\hat{V}_1^{(3)}$	$\hat{V}_1^{(4)}$
p000.q000	2.438(61)	0.449(11)	-0.449(11)					
p100.q100	2.392(72)	0.548(17)	-0.439(13)	0.037(14)	-0.705(22)	0.017(3)	-0.807(24)	-0.119(5)
p100.q000	1.81(46)	0.132(59)	-0.132(59)	1.33(21)	-0.305(97)	0.125(37)	-0.086(51)	0.086(51)
p100.q110	1.63(14)	0.441(49)	-0.023(19)	-0.837(83)	-0.169(57)	-0.036(12)	-0.410(47)	-0.244(24)
p000.q100	1.33(14)	0.299(39)	-0.014(22)	-0.760(79)	-0.088(49)	-0.009(15)	-0.310(47)	-0.217(24)
p100.q200	1.35(22)	0.72(10)	0.047(31)	-0.85(12)	-0.572(12)	0.043(27)	-0.85(13)	-0.315(47)
$aM_0=1.3$								
id.	$\hat{V}_4^{(0)}$	$\hat{V}_4^{(1)}$	$\hat{V}_4^{(2)}$	$\hat{V}_1^{(0)}$	$\hat{V}_1^{(1)}$	$\hat{V}_1^{(2)}$	$\hat{V}_1^{(3)}$	$\hat{V}_1^{(4)}$
p000.q000	2.445(51)	0.525(11)	-0.525(11)					
p100.q100	2.350(61)	0.643(17)	-0.499(12)	0.102(12)	-0.643(17)	0.050(3)	-0.762(20)	-0.169(5)
p100.q000	1.86(41)	0.163(68)	-0.163(68)	1.21(19)	-0.190(83)	0.088(35)	-0.049(44)	0.049(44)
p100.q110	1.43(11)	0.476(47)	-0.058(21)	-0.751(72)	-0.200(46)	0.024(12)	-0.355(40)	-0.242(20)
p000.q100	1.38(13)	0.341(37)	-0.054(22)	-0.742(63)	-0.160(41)	0.042(14)	-0.337(40)	-0.222(21)
p100.q200	1.35(17)	0.741(86)	0.023(26)	-0.711(87)	-0.610(96)	0.126(25)	-0.85(10)	-0.367(42)

TABLE VII. Matrix elements $\hat{V}_\mu^{(i)}$ at $\kappa=0.13769$.

aM_0	$\hat{V}_4^{(0)}$	$\hat{V}_4^{(1)}$	$\hat{V}_4^{(2)}$
5.0	2.78(15)	0.551(31)	-0.551(31)
3.0	2.76(11)	0.578(23)	-0.578(23)
2.1	2.74(10)	0.615(22)	-0.615(22)
1.3	2.721(85)	0.690(20)	-0.690(20)

TABLE VIII. Matrix element $\hat{V}_4^{(i)}$ at $\kappa=0.13816$ for the zero recoil configuration (p000.q000).

κ	0.13630	0.13711	0.13769	0.13816
(0,0,0)	0.48816(62)	0.40756(68)	0.34005(78)	0.2723(11)
(1,0,0)	0.6209(28)	0.5578(44)	0.5065(73)	0.459(15)
(1,1,0)	0.7424(43)	0.6967(71)	0.654(15)	0.626(32)

TABLE IX. Pion energy $aE_\pi(\mathbf{k}_\pi)$ for spatial momenta (0,0,0), (1,0,0), (1,1,0) in unit of $2\pi/La$.

κ	0.13630	0.13711	0.13769	0.13816
$aM_0=5.0$	5.5702(21)	5.5476(29)	5.5318(39)	5.5203(58)
$aM_0=3.0$	3.6606(15)	3.6376(20)	3.6212(27)	3.6088(40)
$aM_0=2.1$	2.7992(12)	2.7758(16)	2.7588(22)	2.7455(32)
$aM_0=1.3$	2.0301(10)	2.0058(13)	1.9883(17)	1.9741(25)

TABLE X. Heavy-light meson mass aM_B evaluated using (6.3) with $\alpha_V(1/a)$.

$aM_0=5.0$				
κ	0.13630	0.13711	0.13769	0.13816
(0,0,0)	0.5887(21)	0.5661(29)	0.5503(39)	0.5388(58)
(1,0,0)	0.6062(15)	0.5821(22)	0.5668(29)	0.5554(40)
$aM_0=3.0$				
κ	0.13630	0.13711	0.13769	0.13816
(0,0,0)	0.5830(15)	0.5600(20)	0.5436(27)	0.5312(40)
(1,0,0)	0.6071(13)	0.5826(17)	0.5665(23)	0.5546(32)
$aM_0=2.1$				
κ	0.13630	0.13711	0.13769	0.13816
(0,0,0)	0.5750(12)	0.5515(16)	0.5346(22)	0.5212(32)
(1,0,0)	0.6054(12)	0.5804(15)	0.5638(20)	0.5512(28)
$aM_0=1.3$				
κ	0.13630	0.13711	0.13769	0.13816
(0,0,0)	0.5571(10)	0.5328(13)	0.5152(17)	0.5010(25)
(1,0,0)	0.5984(12)	0.5711(18)	0.5532(24)	0.5387(35)

TABLE XI. Binding energy of the heavy-light meson $aE_{\text{bin}}(\mathbf{p}_B)$ for spatial momenta (0,0,0) and (1,0,0) in unit of $2\pi/La$.

$C_{1+2}^{(000)}$	$C_{1+2}^{(010)}$	$C_{1+2}^{(100)}$	$C_{1+2}^{(001)}$	$C_{1+2}^{(011)}$	$C_{1+2}^{(002)}$
0.413(74)	3.79(97)	-0.019(31)	-0.53(66)	-3.3(13.8)	0.7(2.3)
0.392(75)	3.94(99)	0.070(29)	-0.59(66)	-3.5(13.8)	0.7(2.3)
$C_2^{(000)}$	$C_2^{(010)}$	$C_2^{(100)}$	$C_2^{(001)}$		
0.311(47)	1.06(1.11)	0.035(37)	-0.06(40)		
0.347(50)	0.99(1.14)	-0.020(37)	-0.04(40)		

TABLE XII. Global fit parameters in the form (6.12)–(6.13). In each column, top and bottom numbers correspond to the result with $\alpha_V(1/a)$ and $\alpha_V(\pi/a)$.

$v \cdot k_\pi$ (GeV)	q^2 (GeV ²)	$f_1(v \cdot k_\pi) + f_2(v \cdot k_\pi)$ (GeV ^{1/2})	$f_2(v \cdot k_\pi)$ (GeV ^{1/2})	$f^0(q^2)$	$f^+(q^2)$	$1/ V_{ub} ^2 d\Gamma/dq^2$ (psec ⁻¹ GeV ⁻²)	
0.1435	26.37	0.98(23)	0.45(20)	0.84(18)	7.4(3.1)	0.0017(15)	
0.1913	25.87	0.95(20)	0.44(19)	0.80(16)	5.5(2.2)	0.021(17)	
0.2392	25.36	0.91(18)	0.44(18)	0.76(15)	4.4(1.6)	0.042(31)	
0.2870	24.86	0.87(17)	0.44(17)	0.73(14)	3.7(1.2)	0.062(41)	
0.3348	24.35	0.83(17)	0.44(15)	0.70(14)	3.18(98)	0.081(50)	
0.3827	23.85	0.79(17)	0.44(14)	0.66(14)	2.78(78)	0.099(56)	
0.4305	23.34	0.76(18)	0.43(13)	0.63(14)	2.46(64)	0.115(60)	
0.4783	22.84	0.73(18)	0.43(12)	0.61(15)	2.21(53)	0.131(62)	
0.5262	22.33	0.69(18)	0.43(11)	0.58(15)	2.00(44)	0.146(64)	
0.5740	21.83	0.66(18)	0.43(10)	0.55(14)	1.82(37)	0.161(65)	
0.6218	21.32	0.64(18)	0.428(93)	0.53(14)	1.67(31)	0.174(65)	
0.6697	20.82	0.61(17)	0.426(88)	0.51(14)	1.54(27)	0.187(66)	*
0.7175	20.31	0.58(17)	0.424(85)	0.49(13)	1.43(24)	0.199(68)	*
0.7653	19.81	0.56(15)	0.422(84)	0.47(12)	1.33(22)	0.210(71)	*
0.8132	19.30	0.54(14)	0.421(86)	0.45(11)	1.24(21)	0.221(76)	*
0.8610	18.80	0.52(13)	0.419(90)	0.435(98)	1.16(21)	0.231(84)	*
0.9088	18.29	0.50(12)	0.417(97)	0.421(92)	1.09(21)	0.240(94)	*
0.9567	17.79	0.48(11)	0.42(10)	0.407(92)	1.03(22)	0.25(11)	*
1.0045	17.28	0.47(13)	0.41(11)	0.40(10)	0.97(23)	0.26(13)	
1.0523	16.78	0.45(15)	0.41(12)	0.38(12)	0.92(25)	0.27(15)	
1.1002	16.27	0.44(19)	0.41(14)	0.38(15)	0.87(27)	0.27(17)	
1.1480	15.77	0.43(24)	0.41(15)	0.37(18)	0.83(29)	0.28(20)	

TABLE XIII. Numerical results for the form factors and for the differential decay rate. Error contains the statistical and estimated systematic uncertainties. Results with a * symbol in the last column are those obtained by interpolating the lattice data in $v \cdot k_\pi$, while others involve an extrapolation.

FIGURES

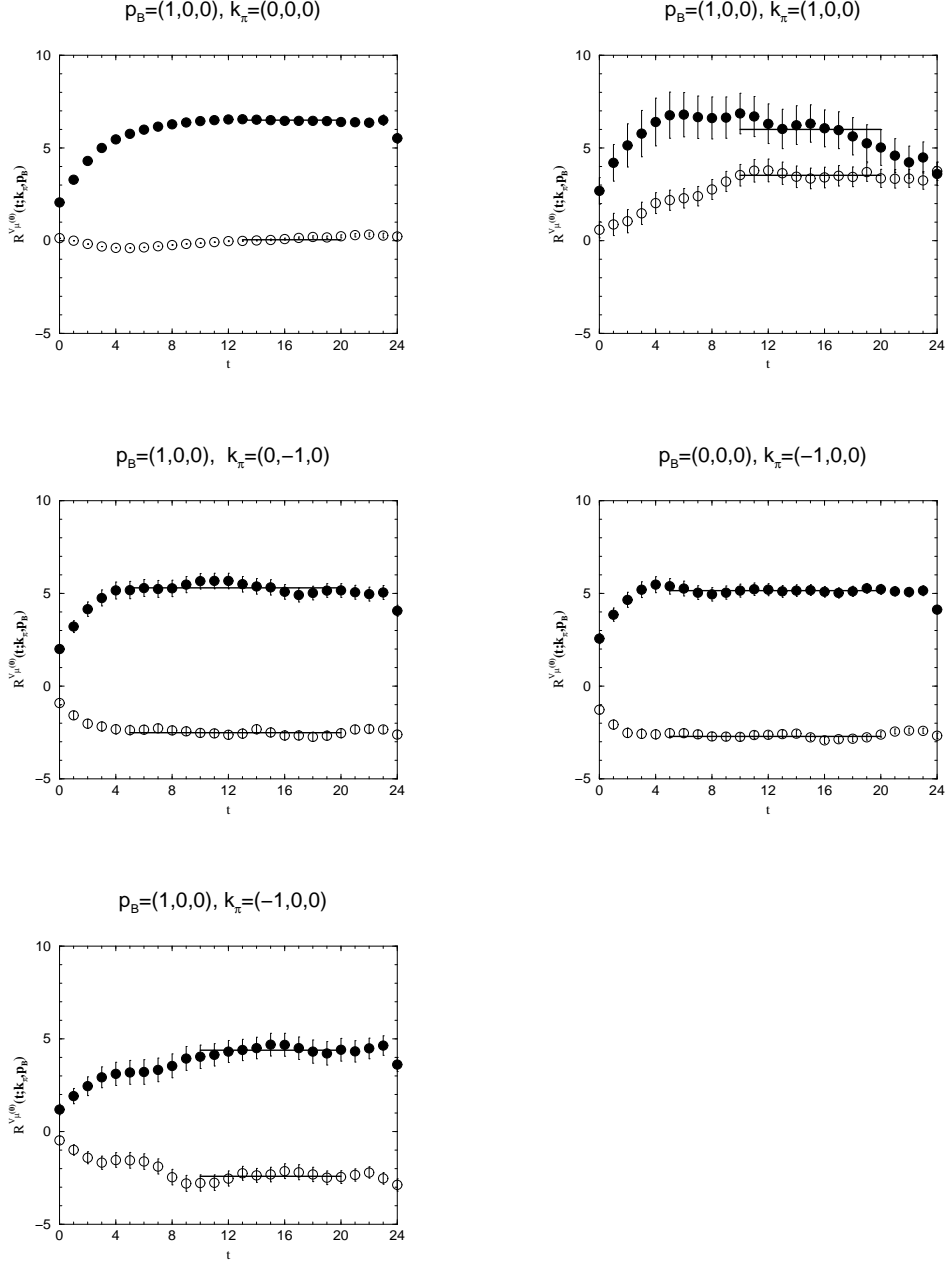


FIG. 1. Ratio $R^{V_\mu^{(i)}}(t; \mathbf{k}_\pi, \mathbf{p}_B)$ for five combinations of \mathbf{k}_π and \mathbf{p}_B . Filled symbols represent the ratio for $V_4^{(0)}$, and open symbols are for $V_1^{(0)}$. Light quark is at $\kappa=0.13711$, and the heavy quark mass roughly corresponds to the b quark mass, i.e. $aM_0=3.0$.

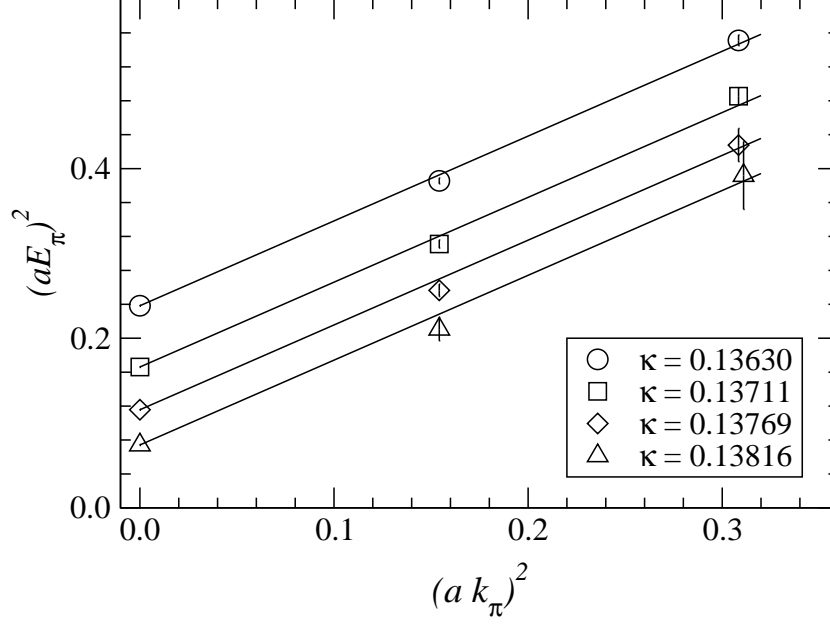


FIG. 2. Dispersion relation for pion. The lines represent the continuum form (6.1).

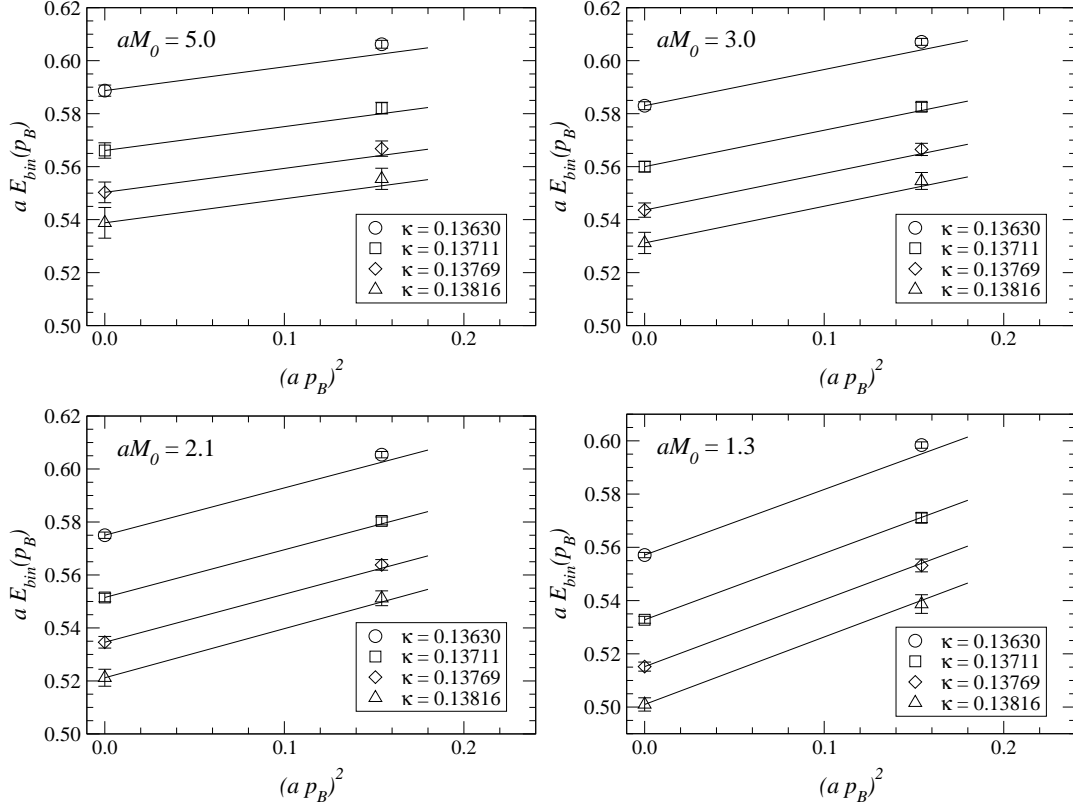


FIG. 3. Dispersion relation for the heavy-light meson at $aM_0 = 5.0, 3.0, 2.1$ and 1.3 . The lines represent the non-relativistic form (6.2) with perturbatively calculated meson mass aM_B .

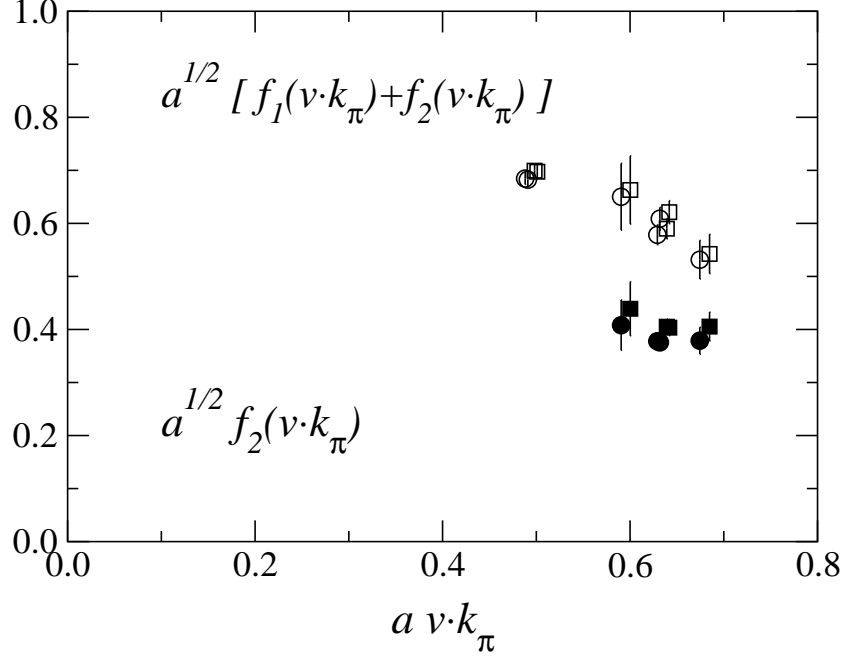


FIG. 4. A typical plot of the form factors $f_1(v \cdot k_\pi) + f_2(v \cdot k_\pi)$ (open symbols) and $f_2(v \cdot k_\pi)$ (filled symbols) in the lattice unit. Parameters are $aM_0=3.0$, $\kappa=0.13630$, and $\alpha_V(1/a)$ (circles) or $\alpha_V(\pi/a)$ (squares) are used for the perturbative matching. The data for $\alpha_V(\pi/a)$ is slightly shifted in horizontal direction for clarity.

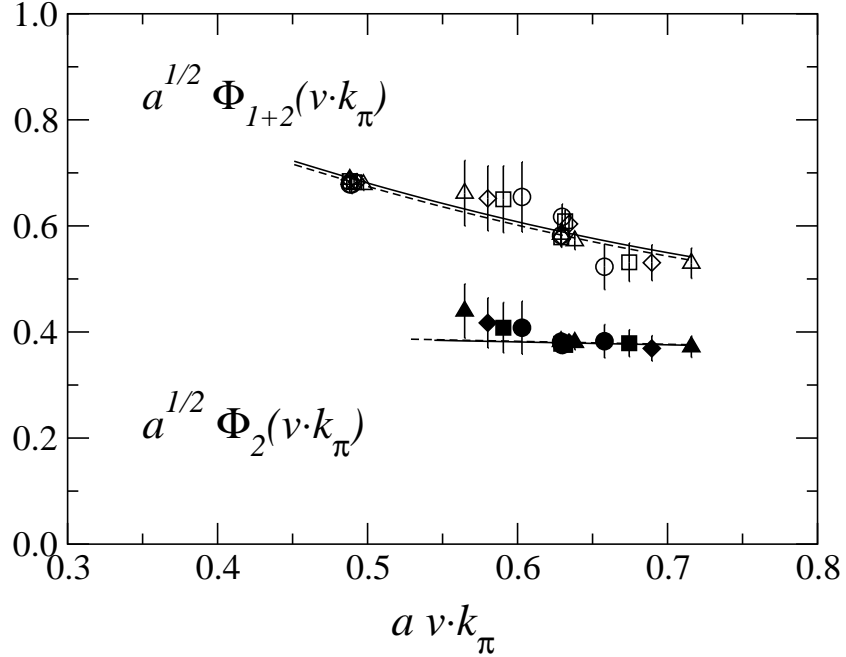


FIG. 5. The renormalization group invariant form factors $\Phi_{1+2}(v \cdot k_\pi)$ (open symbols) and $\Phi_2(v \cdot k_\pi)$ (filled symbols) for different values of aM_0 with fixed light quark mass $\kappa=0.13630$. Symbols denote the data at $aM_0=5.0$ (circles), 3.0 (squares), 2.1 (diamonds) and 1.3 (triangles). Solid and dashed lines show the fit (6.12)–(6.13) for the heaviest ($aM_0=5.0$) and the lightest ($aM_0=1.3$) heavy quark masses respectively.

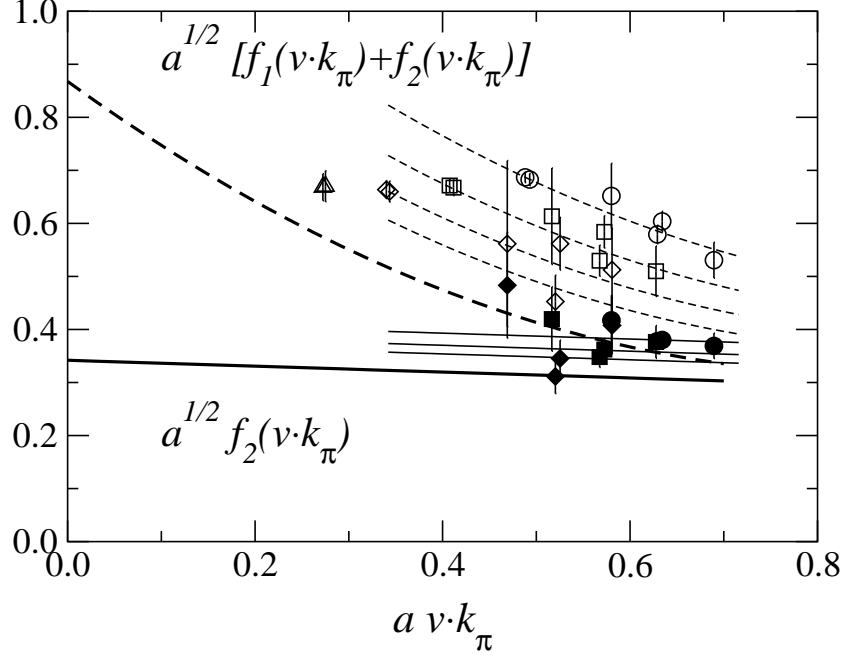


FIG. 6. Light quark mass dependence of $f_1(v \cdot k_\pi) + f_2(v \cdot k_\pi)$ (open symbols) and $f_2(v \cdot k_\pi)$ (filled symbols) for $aM_0=2.1$. Symbols denote the data at $\kappa=0.13630$ (circles), 0.13711 (squares), 0.13769 (diamonds) and 0.13816 (triangles). Three thin solid lines, from above to below, show the fit (6.13) for $f_2(v \cdot k_\pi)$ with three κ values, from heaviest to lightest. Four thin dashed lines, on the other hand, correspond to the fit (6.12) for the data of $f_1(v \cdot k_\pi) + f_2(v \cdot k_\pi)$ for four values of κ . Thick lines represent the limit of physical light quark mass.

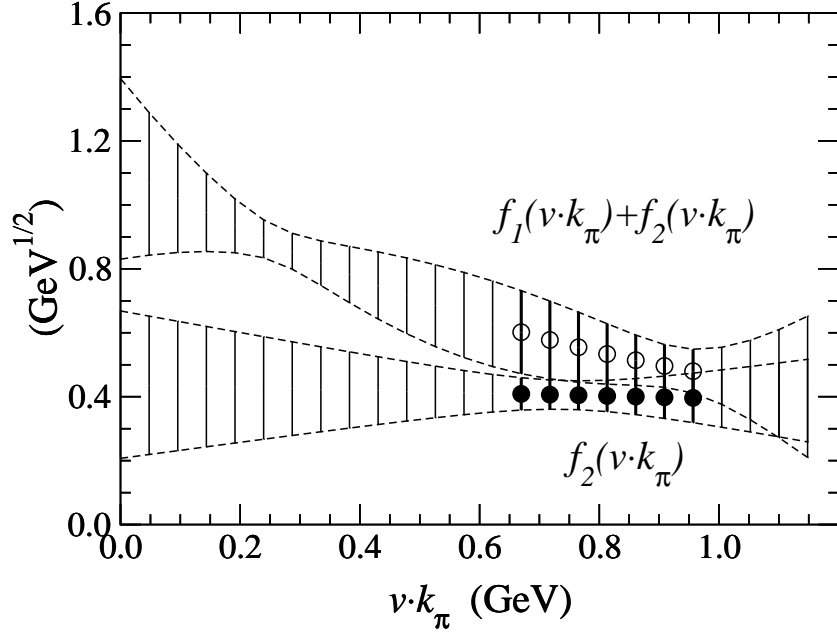


FIG. 7. Form factors $f_1(v \cdot k_\pi) + f_2(v \cdot k_\pi)$ (open symbols) and $f_2(v \cdot k_\pi)$ (filled symbols) at physical mass parameters. The points with symbols are obtained by interpolation in $v \cdot k_\pi$, while others involve extrapolations.

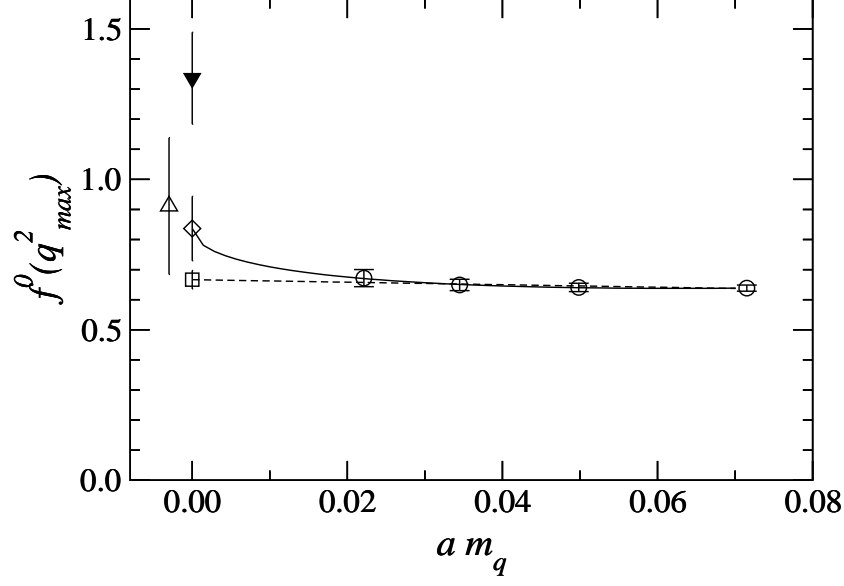


FIG. 8. Soft pion limit of $f_0(q_{max}^2) = \frac{2}{\sqrt{m_B}}[f_1(v \cdot k_\pi) + f_2(v \cdot k_\pi)]$ at $aM_0=3.0$. The dashed line is a linear fit in $(am_\pi)^2$, while the solid curve includes the term (am_π) . A result of the fit (6.12) is given by an open triangle, which should be equal to f_B/f_π (filled triangle) in the soft pion theorem.

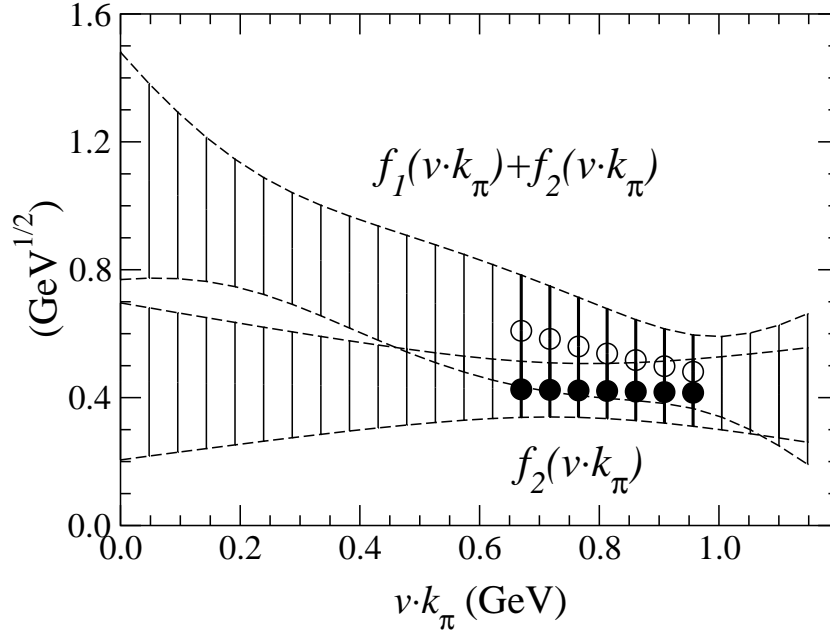


FIG. 9. Same as Figure 7, but with estimated systematic errors.

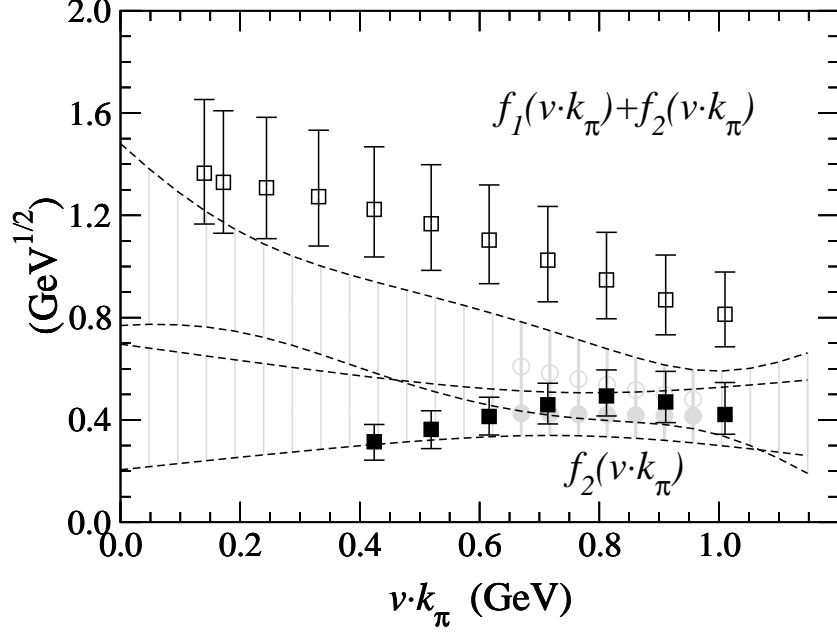


FIG. 10. Form factors $f_1(v \cdot k_{\pi}) + f_2(v \cdot k_{\pi})$ (open symbols) and $f_2(v \cdot k_{\pi})$ (filled symbols) at physical mass parameters. Squares represent the results of [11], while our data presented in Figure 7 is now plotted with gray symbols.

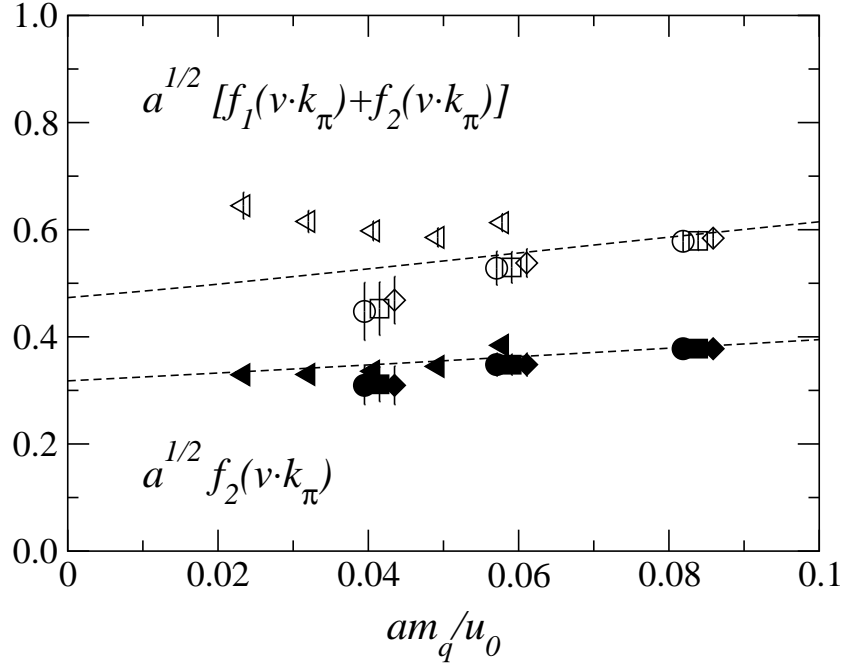


FIG. 11. Form factors $f_1(v \cdot k_{\pi}) + f_2(v \cdot k_{\pi})$ (open symbols) and $f_2(v \cdot k_{\pi})$ (filled symbols) for a fixed momentum configuration $a\mathbf{p}_B = (0, 0, 0)$ and $a\mathbf{k}_{\pi} = (1, 0, 0)$ are plotted as a function of light quark mass am_q/u_0 . Triangles are results of the Fermilab group [11] for a heavy quark mass close to the b quark mass. Our results are shown for $aM_0 = 3.0$ (circles), 2.1 (squares) and 1.3 (diamonds). Squares and diamonds are shifted in the horizontal direction for clarity. Lines show the global fit (6.12) and (6.13).

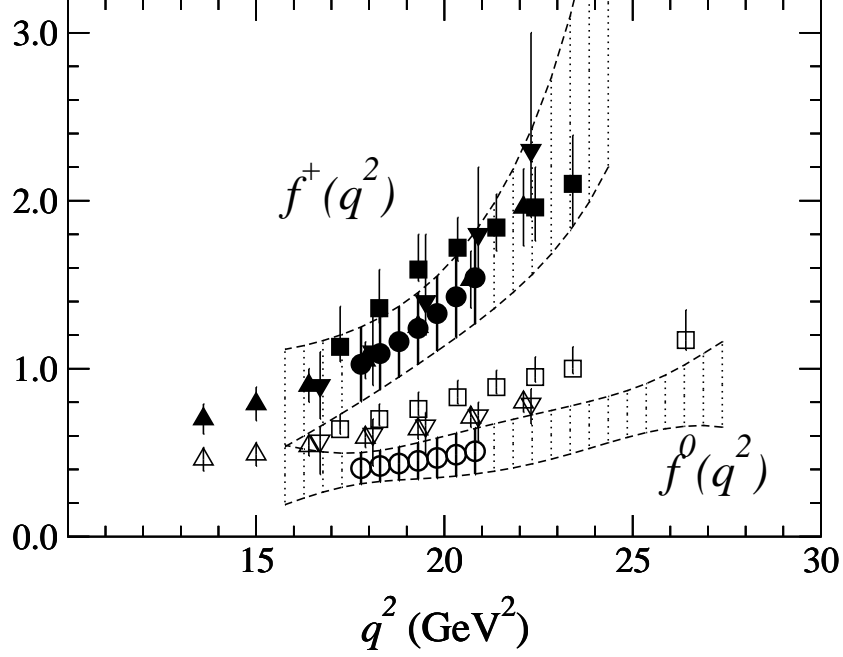


FIG. 12. Comparison of the results for the form factors $f^+(q^2)$ (filled symbols) and $f^0(q^2)$ (open symbols). Data are from APE [7] (up triangles), UKQCD [6] (down triangles) and Fermilab [11] (squares). Our results are plotted by circles and error bands are shown by dashed lines.

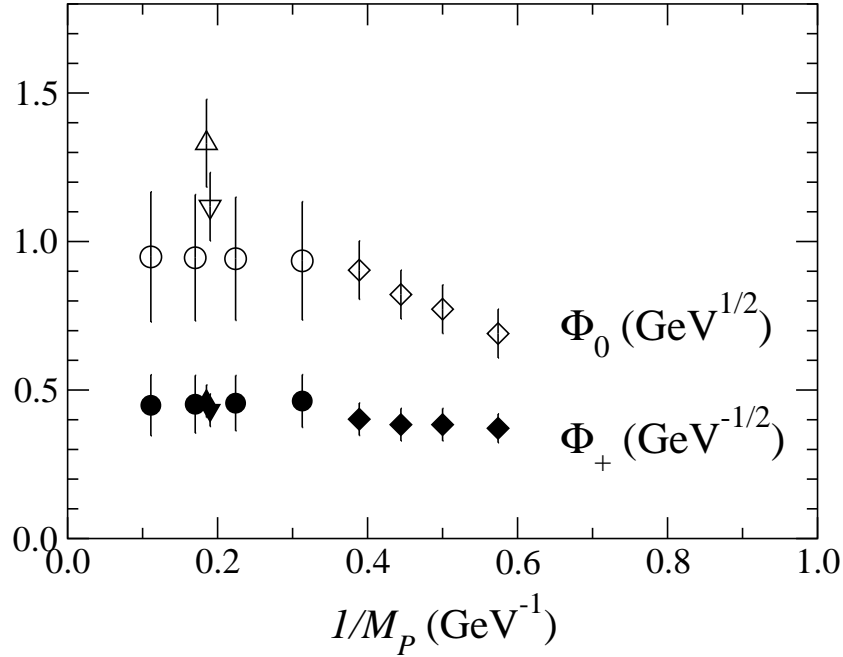


FIG. 13. $1/M_P$ dependence of the form factors $\Phi_+ \equiv (\alpha_s(M_P)/\alpha_s(M_B))^{-2/11} f^+/\sqrt{M_P}$ (filled symbols) $\Phi_0 \equiv (\alpha_s(M_P)/\alpha_s(M_B))^{-2/11} f^0\sqrt{M_P}$ (open symbols) at a fixed $v \cdot k_\pi (= 0.845 \text{ GeV})$. Simulation results from the APE collaboration [7] are shown by diamonds, and their linear and quadratic extrapolation to the B meson mass is plotted by down and up triangles, respectively. Our results are given by circles.

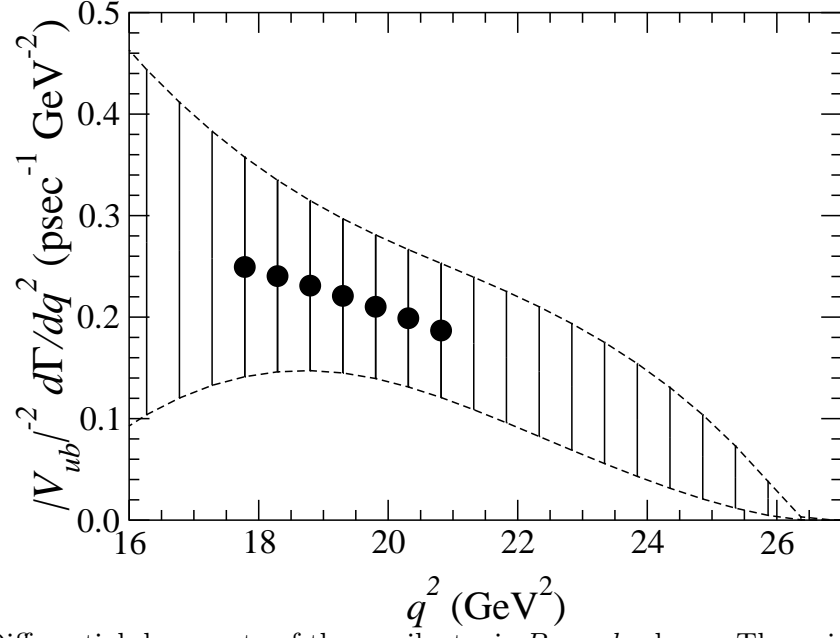


FIG. 14. Differential decay rate of the semileptonic $B \rightarrow \pi l \nu$ decay. The points with symbols are obtained by interpolation in $v \cdot k_\pi$, while others involve extrapolations.